Beamforming in the Time Domain

J. Benesty, I. Cohen, and J. Chen,
Fundamentals of Signal Enhancement and Array Signal Processing,
Wiley-IEEE Press, 2017.

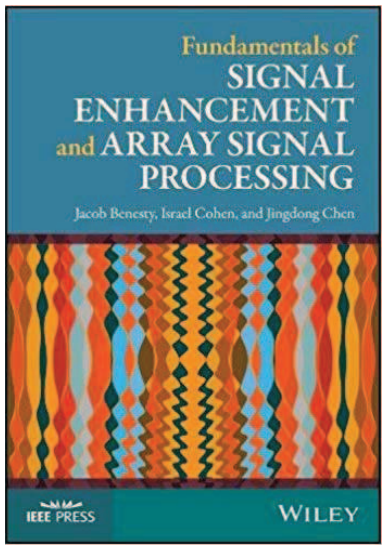

Outline

Introduction

This talk is concerned with beamforming in the time domain, which has the advantage to be more intuitive than beamforming in the frequency domain.

Furthermore, the approach depicted here is broadband in nature.

We describe the time-domain signal model that we adopt and explain how broadband beamforming works.

Then, we define many performance measures, which are essential for the derivation and analysis of broadband beamformers.

We show how to derive fixed and adaptive time-domain beamformers.

Signal Model and Problem Formulation

We consider a desired broadband source signal, $x(t)$, in the far-field that propagates in an anechoic acoustic environment, and impinges on a ULA consisting of M omnidirectional sensors, where the distance between two successive sensors is equal to δ (see Fig. 1).

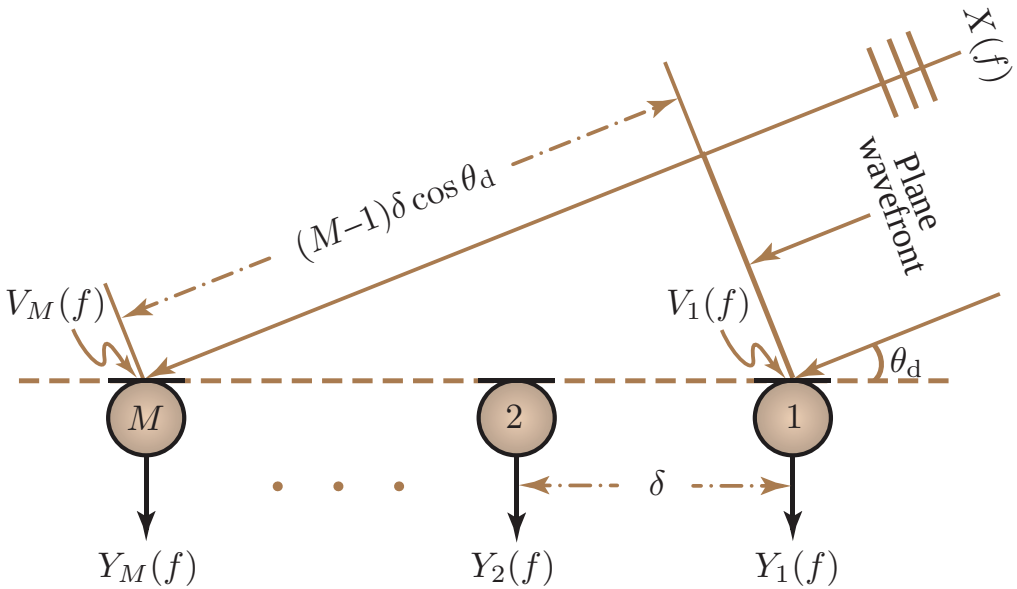

Figure 1: A uniform linear array with M sensors.

In the rest, sensor 1 is chosen as the reference.

In this scenario, the signal measured at the mth sensor is given by [1]

$$\begin{aligned} y_m(t) &= x\left[t - \Delta - f_{\mathrm{s}}\tau_m\left(\cos\theta_{\mathrm{d}}\right)\right] + v_m(t) \\ &= x_m(t) + v_m(t),\ m = 1, 2, \ldots, M, \end{aligned} \tag{1}$$

where Δ is the propagation time from the position of the source (desired signal), $x(t)$, to sensor 1, f_{s} is the sampling frequency,

$$\tau_m\left(\cos\theta_{\mathrm{d}}\right) = (m-1)\frac{\delta\cos\theta_{\mathrm{d}}}{c} \tag{2}$$

is the delay between the first and mth sensors, θ_{d} is the direction of the desired signal, c is the speed of the waves in the medium, and $v_m(t)$ is the noise picked up by the mth sensor.

For the sake of simplicity, we assume that

$$0 \leq \frac{f_{\mathrm{s}} \delta \cos \theta_{\mathrm{d}}}{c} \in \mathbb{Z}. \tag{3}$$

This clearly restricts θ_{d}, but simplifies the signal model.

In the sequel, we generalize the signal model when assumption (3) is not satisfied. Under this assumption, we can express (1) as

$$y_m(t) = \mathbf{g}_m^T \left(\cos \theta_{\mathrm{d}}\right) \mathbf{x}' \left(t - \Delta\right) + v_m(t), \tag{4}$$

where

$$\mathbf{g}_m \left(\cos \theta_{\mathrm{d}}\right) = \begin{bmatrix} 0 & \cdots & 0 & 1 & 0 & \cdots & 0 \end{bmatrix}^T \tag{5}$$

is a vector of length $L_g \geq f_s \tau_m (\cos\theta_d) + 1$ whose $[f_s \tau_m (\cos\theta_d) + 1]$th component is equal to 1 and

$$\mathbf{x}'(t-\Delta) = \left[\begin{array}{cccc} x(t-\Delta) & x(t-\Delta-1) & \cdots & \\ & x[t-\Delta-f_s\tau_m(\cos\theta_d)] & \cdots & x(t-\Delta-L_g+1) \end{array} \right]^T. \tag{6}$$

The vector $\mathbf{g}_m(\cos\theta_d)$ is a 1-sparse vector and the position of the 1 depends on both θ_d and m, with

$$\mathbf{g}_1(\cos\theta_d) = \left[\begin{array}{cccc} 1 & 0 & \cdots & 0 \end{array} \right]^T. \tag{7}$$

By considering L_h successive time samples of the mth sensor signal, (4) becomes a vector of length L_h:

$$\mathbf{y}_m(t) = \mathbf{G}_m(\cos\theta_d)\,\mathbf{x}(t-\Delta) + \mathbf{v}_m(t), \tag{8}$$

where

$$\mathbf{G}_m\left(\cos\theta_{\mathrm{d}}\right) = \begin{bmatrix} \mathbf{g}_m^T\left(\cos\theta_{\mathrm{d}}\right) & 0 & 0 & \cdots & 0 \\ 0 & \mathbf{g}_m^T\left(\cos\theta_{\mathrm{d}}\right) & 0 & \cdots & 0 \\ \vdots & \vdots & \ddots & & \vdots \\ 0 & 0 & 0 & \cdots & \mathbf{g}_m^T\left(\cos\theta_{\mathrm{d}}\right) \end{bmatrix} \tag{9}$$

is a Sylvester matrix of size $L_h \times L$, with $L = L_g + L_h - 1$,

$$\mathbf{x}\left(t-\Delta\right) = \begin{bmatrix} x\left(t-\Delta\right) & x\left(t-\Delta-1\right) & \cdots & x\left(t-\Delta-L+1\right) \end{bmatrix}^T \tag{10}$$

is a vector of length L, and

$$\mathbf{v}_m(t) = \begin{bmatrix} v_m(t) & v_m(t-1) & \cdots & v_m(t-L_h+1) \end{bmatrix}^T. \tag{11}$$

Figure 2 illustrates the multichannel signal model in the time domain.

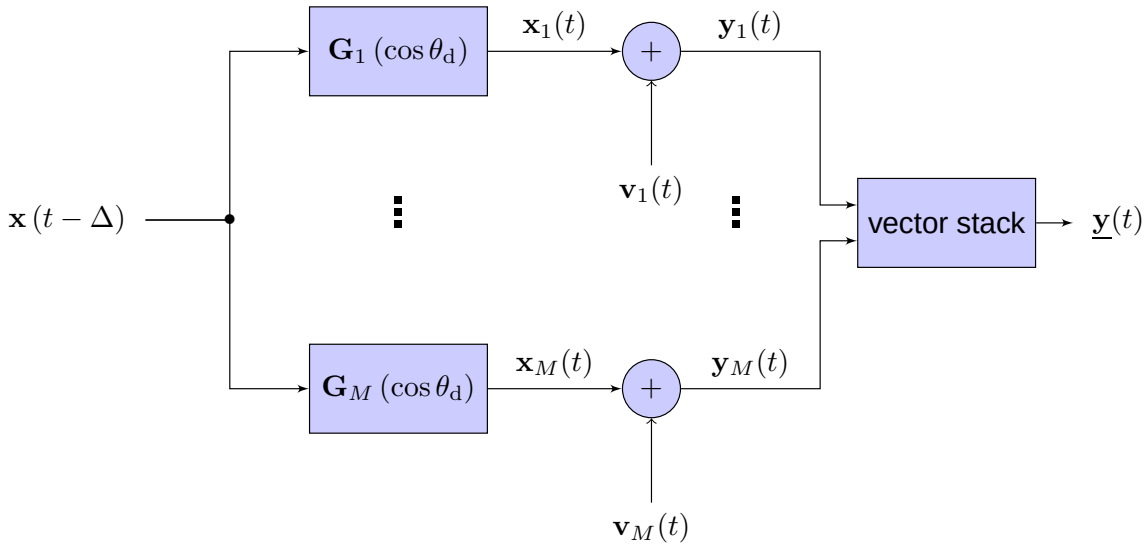

Figure 2: Multichannel signal model in the time domain.

By concatenating the observations from the M sensors, we get the vector of length ML_h:

$$\begin{aligned}\underline{\mathbf{y}}(t) &= \left[\begin{array}{cccc}\mathbf{y}_1^T(t) & \mathbf{y}_2^T(t) & \cdots & \mathbf{y}_M^T(t)\end{array}\right]^T \\ &= \underline{\mathbf{G}}\left(\cos\theta_{\mathrm{d}}\right)\mathbf{x}\left(t-\Delta\right)+\underline{\mathbf{v}}(t) \\ &= \underline{\mathbf{x}}(t)+\underline{\mathbf{v}}(t),\end{aligned} \tag{12}$$

where

$$\underline{\mathbf{G}}\left(\cos\theta_{\mathrm{d}}\right) = \left[\begin{array}{c}\mathbf{G}_1\left(\cos\theta_{\mathrm{d}}\right) \\ \mathbf{G}_2\left(\cos\theta_{\mathrm{d}}\right) \\ \vdots \\ \mathbf{G}_M\left(\cos\theta_{\mathrm{d}}\right)\end{array}\right] \tag{13}$$

is a matrix of size $ML_h \times L$,

$$\underline{\mathbf{v}}(t) = \left[\begin{array}{cccc}\mathbf{v}_1^T(t) & \mathbf{v}_2^T(t) & \cdots & \mathbf{v}_M^T(t)\end{array}\right]^T \tag{14}$$

is a vector of length ML_h, and

$$\begin{aligned}\underline{\mathbf{x}}(t) &= \left[\begin{array}{cccc}\mathbf{x}_1^T(t) & \mathbf{x}_2^T(t) & \cdots & \mathbf{x}_M^T(t)\end{array}\right]^T \\ &= \underline{\mathbf{G}}\left(\cos\theta_{\mathrm{d}}\right)\mathbf{x}\left(t-\Delta\right), \end{aligned} \tag{15}$$

with $\mathbf{x}_m(t) = \mathbf{G}_m\left(\cos\theta_{\mathrm{d}}\right)\mathbf{x}\left(t-\Delta\right)$.

From (12), we deduce that the correlation matrix (of size $ML_h \times ML_h$) of $\underline{\mathbf{y}}(t)$ is

$$\begin{aligned}\mathbf{R}_{\underline{\mathbf{y}}} &= E\left[\underline{\mathbf{y}}(t)\underline{\mathbf{y}}^T(t)\right] \\ &= \mathbf{R}_{\underline{\mathbf{x}}} + \mathbf{R}_{\underline{\mathbf{v}}} \\ &= \underline{\mathbf{G}}\left(\cos\theta_{\mathrm{d}}\right)\mathbf{R}_{\mathbf{x}}\underline{\mathbf{G}}^T\left(\cos\theta_{\mathrm{d}}\right) + \mathbf{R}_{\underline{\mathbf{v}}}, \end{aligned} \tag{16}$$

where $\mathbf{R}_{\underline{\mathbf{x}}}$, $\mathbf{R}_{\underline{\mathbf{v}}}$, and $\mathbf{R}_{\mathbf{x}}$ are the correlation matrices of $\underline{\mathbf{x}}(t)$, $\underline{\mathbf{v}}(t)$, and $\mathbf{x}\left(t-\Delta\right)$, respectively.

We always assume that $\mathbf{R}_{\underline{\mathbf{v}}}$ has full rank.

But, to fully exploit the spatial information like in the frequency domain, the matrix $\mathbf{R}_{\underline{\mathbf{x}}} = \underline{\mathbf{G}}\left(\cos\theta_{\mathrm{d}}\right)\mathbf{R}_{\mathbf{x}}\underline{\mathbf{G}}^{T}\left(\cos\theta_{\mathrm{d}}\right)$ must be rank deficient.

Since the size of $\underline{\mathbf{G}}\left(\cos\theta_{\mathrm{d}}\right)$ is $ML_h \times L$ and the size of $\mathbf{R}_{\mathbf{x}}$ is $L \times L$, the condition for that is

$$ML_h > L \tag{17}$$

or, equivalently,

$$L_h > \frac{L_g - 1}{M - 1}. \tag{18}$$

We see that as M is increased, the minimal value of L_h is decreased.

Then, our objective is to design all kind of time-domain or broadband beamformers with a real-valued spatiotemporal filter of length ML_h:

$$\underline{\mathbf{h}} = \left[\begin{array}{cccc} \mathbf{h}_1^T & \mathbf{h}_2^T & \cdots & \mathbf{h}_M^T \end{array} \right]^T, \tag{19}$$

where $\mathbf{h}_m,\ m = 1, 2, \ldots, M$ are temporal filters of length L_h.

To generalize the signal model when assumption (3) is not satisfied, we resort to Shannon's sampling theorem [2], [3], which implies that

$$x_m(t) = x\left[t - \Delta - f_{\mathrm{s}}\tau_m\left(\cos\theta_{\mathrm{d}}\right)\right] \tag{20}$$

$$= \sum_{n=-\infty}^{\infty} x\left(t - \Delta - n\right) \operatorname{sinc}\left[n - f_{\mathrm{s}}\tau_m\left(\cos\theta_{\mathrm{d}}\right)\right] \tag{21}$$

and for $P \gg f_{\mathrm{s}}\tau_m\left(\cos\theta_{\mathrm{d}}\right)$ we have

$$x_m(t) \approx \sum_{n=-P-L_h+1}^{P} x\left(t-\Delta-n\right)\operatorname{sinc}\left[n-f_{\mathrm{s}}\tau_m\left(\cos\theta_{\mathrm{d}}\right)\right]. \tag{22}$$

Hence, we can simply redefine $\mathbf{x}\left(t-\Delta\right)$ as a vector of length $L=2P+L_h$ with

$$\mathbf{x}\left(t-\Delta\right) = \left[\begin{array}{cc} x\left(t-\Delta+P+L_h-1\right) & x\left(t-\Delta+P+L_h-2\right) \\ \cdots & x\left(t-\Delta-P\right) \end{array}\right]^T \tag{23}$$

and redefine $\mathbf{G}_m\left(\cos\theta_{\mathrm{d}}\right)$ as a Toeplitz matrix of size $L_h \times L$ with:

$$\left[\mathbf{G}_m\left(\cos\theta_{\mathrm{d}}\right)\right]_{i,j} = \operatorname{sinc}\left[-P-L_h+1-i+j-f_{\mathrm{s}}\tau_m\left(\cos\theta_{\mathrm{d}}\right)\right], \tag{24}$$

where $i=1,\ldots,L_h$, $j=1,\ldots,L$.

Broadband Beamforming

By applying the spatiotemporal filter, $\underline{\mathbf{h}}$, to the observation signal vector, $\underline{\mathbf{y}}(t)$, we obtain the output of the broadband beamformer, as illustrated in Fig. 3:

$$\begin{aligned} z(t) &= \sum_{m=1}^{M} \mathbf{h}_m^T \mathbf{y}_m(t) \\ &= \underline{\mathbf{h}}^T \underline{\mathbf{y}}(t) \\ &= x_{\mathrm{fd}}(t) + v_{\mathrm{rn}}(t). \end{aligned} \tag{25}$$

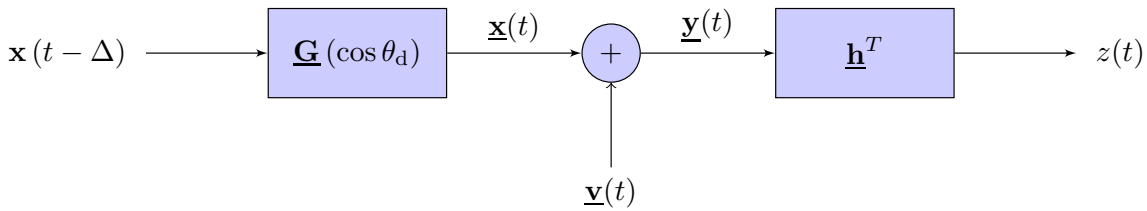

Figure 3: Block diagram of broadband beamforming in the time domain.

The filtered desired signal is given by

$$x_{\mathrm{fd}}(t) = \sum_{m=1}^{M} \mathbf{h}_m^T \mathbf{G}_m \left(\cos\theta_{\mathrm{d}}\right) \mathbf{x}\left(t-\Delta\right) \tag{26}$$
$$= \underline{\mathbf{h}}^T \underline{\mathbf{G}} \left(\cos\theta_{\mathrm{d}}\right) \mathbf{x}\left(t-\Delta\right)$$

is and

$$v_{\mathrm{rn}}(t) = \sum_{m=1}^{M} \mathbf{h}_m^T \mathbf{v}_m(t) \tag{27}$$
$$= \underline{\mathbf{h}}^T \underline{\mathbf{v}}(t)$$

is the residual noise.

We deduce that the variance of $z(t)$ is

$$\begin{aligned}\sigma_z^2 &= \underline{\mathbf{h}}^T \mathbf{R}_{\underline{\mathbf{y}}} \underline{\mathbf{h}} \\ &= \sigma_{x_{\mathrm{fd}}}^2 + \sigma_{v_{\mathrm{rn}}}^2,\end{aligned} \tag{28}$$

where

$$\begin{aligned}\sigma_{x_{\mathrm{fd}}}^2 &= \underline{\mathbf{h}}^T \underline{\mathbf{G}} \left(\cos\theta_{\mathrm{d}}\right) \mathbf{R}_{\mathbf{x}} \underline{\mathbf{G}}^T \left(\cos\theta_{\mathrm{d}}\right) \underline{\mathbf{h}} \\ &= \underline{\mathbf{h}}^T \mathbf{R}_{\underline{\mathbf{x}}} \underline{\mathbf{h}}\end{aligned} \tag{29}$$

is the variance of $x_{\mathrm{fd}}(t)$ and

$$\sigma_{v_{\mathrm{rn}}}^2 = \underline{\mathbf{h}}^T \mathbf{R}_{\underline{\mathbf{v}}} \underline{\mathbf{h}} \tag{30}$$

is the variance of $v_{\mathrm{rn}}(t)$.

In principle, any element of the vector $\mathbf{x}(t-\Delta)$ can be considered as the desired signal.

Therefore, from (26), we see that the distortionless constraint is

$$\underline{\mathbf{h}}^T \underline{\mathbf{G}}(\cos\theta_{\mathrm{d}}) = \mathbf{i}_l^T, \tag{31}$$

where $\mathbf{i}_l$ is the lth column of the $L \times L$ identity matrix, $\mathbf{I}_L$.

Performance Measures
Signal-to-Noise Ratio

In this section, we define all relevant performance measures for the derivation and analysis of fixed and adaptive beamformers in the time domain.

For fixed beamforming only, since we are concerned with broadband signals, we assume for convenience that the source signal, $x(t)$, is white; this way, the whole spectrum is taken into account.

Since sensor 1 is the reference, the input SNR is computed from the first L_h components of $\underline{\mathbf{y}}(t)$ as defined in (12), i.e., $\mathbf{y}_1(t) = \mathbf{x}_1(t) + \mathbf{v}_1(t)$.

We easily find that

$$\begin{aligned} \text{iSNR} &= \frac{\text{tr}\left(\mathbf{R}_{\mathbf{x}_1}\right)}{\text{tr}\left(\mathbf{R}_{\mathbf{v}_1}\right)} \\ &= \frac{\sigma_x^2}{\sigma_{v_1}^2}, \end{aligned} \tag{32}$$

where $\mathbf{R}_{\mathbf{x}_1}$ and $\mathbf{R}_{\mathbf{v}_1}$ are the correlation matrices of $\mathbf{x}_1(t)$ and $\mathbf{v}_1(t)$, respectively, and σ_x^2 and $\sigma_{v_1}^2$ are the variances of $x(t)$ and $v_1(t)$, respectively.

The output SNR is obtained from (28).

It is given by

$$\begin{aligned}\mathrm{oSNR}\left(\underline{\mathbf{h}}\right) &= \frac{\sigma_{x_{\mathrm{fd}}}^2}{\sigma_{v_{\mathrm{rn}}}^2} \\ &= \frac{\underline{\mathbf{h}}^T \underline{\mathbf{G}} \left(\cos\theta_{\mathrm{d}}\right) \mathbf{R}_{\mathbf{x}} \underline{\mathbf{G}}^T \left(\cos\theta_{\mathrm{d}}\right) \underline{\mathbf{h}}}{\underline{\mathbf{h}}^T \mathbf{R}_{\underline{\mathbf{v}}} \underline{\mathbf{h}}} \\ &= \frac{\sigma_x^2}{\sigma_{v_1}^2} \times \frac{\underline{\mathbf{h}}^T \underline{\mathbf{G}} \left(\cos\theta_{\mathrm{d}}\right) \underline{\mathbf{G}}^T \left(\cos\theta_{\mathrm{d}}\right) \underline{\mathbf{h}}}{\underline{\mathbf{h}}^T \mathbf{\Gamma}_{\underline{\mathbf{v}}} \underline{\mathbf{h}}},\end{aligned} \tag{33}$$

where

$$\mathbf{\Gamma}_{\underline{\mathbf{v}}} = \frac{\mathbf{R}_{\underline{\mathbf{v}}}}{\sigma_{v_1}^2} \tag{34}$$

is the pseudo-correlation matrix of $\underline{\mathbf{v}}(t)$.

The third line of (33) is valid for fixed beamforming only.

White Noise Gain

We see from (33) that the array gain is

$$\mathcal{G}\left(\underline{\mathbf{h}}\right) = \frac{\mathrm{oSNR}\left(\underline{\mathbf{h}}\right)}{\mathrm{iSNR}} = \frac{\underline{\mathbf{h}}^T \underline{\mathbf{G}} \left(\cos\theta_{\mathrm{d}}\right) \underline{\mathbf{G}}^T \left(\cos\theta_{\mathrm{d}}\right) \underline{\mathbf{h}}}{\underline{\mathbf{h}}^T \mathbf{\Gamma}_{\underline{\mathbf{v}}} \underline{\mathbf{h}}}. \tag{35}$$

The white noise gain (WNG) is obtained by taking $\mathbf{\Gamma}_{\underline{\mathbf{v}}} = \mathbf{I}_{ML_h}$ in (35), where $\mathbf{I}_{ML_h}$ is the $ML_h \times ML_h$ identity matrix, i.e.,

$$\mathcal{W}\left(\underline{\mathbf{h}}\right) = \frac{\underline{\mathbf{h}}^T \underline{\mathbf{G}} \left(\cos\theta_{\mathrm{d}}\right) \underline{\mathbf{G}}^T \left(\cos\theta_{\mathrm{d}}\right) \underline{\mathbf{h}}}{\underline{\mathbf{h}}^T \underline{\mathbf{h}}}. \tag{36}$$

Directivity Factor

We define the broadband beampattern or broadband directivity pattern as

$$\left|\mathcal{B}\left(\underline{\mathbf{h}}, \cos\theta\right)\right|^2 = \underline{\mathbf{h}}^T \underline{\mathbf{G}}\left(\cos\theta\right) \underline{\mathbf{G}}^T\left(\cos\theta\right) \underline{\mathbf{h}}. \tag{37}$$

In the time domain, the definition of the directivity factor (DF) is

$$\begin{aligned} \mathcal{D}\left(\underline{\mathbf{h}}\right) &= \frac{\left|\mathcal{B}\left(\underline{\mathbf{h}}, \cos\theta_{\mathrm{d}}\right)\right|^2}{\frac{1}{2}\int_0^{\pi} \left|\mathcal{B}\left(\underline{\mathbf{h}}, \cos\theta\right)\right|^2 \sin\theta d\theta} \\ &= \frac{\underline{\mathbf{h}}^T \underline{\mathbf{G}}\left(\cos\theta_{\mathrm{d}}\right) \underline{\mathbf{G}}^T\left(\cos\theta_{\mathrm{d}}\right) \underline{\mathbf{h}}}{\underline{\mathbf{h}}^T \mathbf{\Gamma}_{\mathrm{T},0,\pi} \underline{\mathbf{h}}}, \end{aligned} \tag{38}$$

where

$$\mathbf{\Gamma}_{\mathrm{T},0,\pi} = \frac{1}{2}\int_0^{\pi} \underline{\mathbf{G}}\left(\cos\theta\right)\underline{\mathbf{G}}^T\left(\cos\theta\right)\sin\theta d\theta \tag{39}$$

is a matrix of size $ML_h \times ML_h$, which is the equivalent form of $\mathbf{\Gamma}_{0,\pi}(f)$ in the time domain.

Note that an explicit expression for $\mathbf{\Gamma}_{\mathrm{T},0,\pi}$ is not available.

In practice, we compute the DF in the time domain directly from the first line of (38) with numerical integration.

Front-to-Back Ratio

In the same manner, we define the broadband front-to-back ratio (FBR) as

$$\mathcal{F}\left(\underline{\mathbf{h}}\right) = \frac{\frac{1}{2}\int_0^{\pi/2} \left|\mathcal{B}\left(\underline{\mathbf{h}}, \cos\theta\right)\right|^2 \sin\theta d\theta}{\frac{1}{2}\int_{\pi/2}^{\pi} \left|\mathcal{B}\left(\underline{\mathbf{h}}, \cos\theta\right)\right|^2 \sin\theta d\theta} \tag{40}$$

$$= \frac{\underline{\mathbf{h}}^T \mathbf{\Gamma}_{\mathrm{T},0,\pi/2} \underline{\mathbf{h}}}{\underline{\mathbf{h}}^T \mathbf{\Gamma}_{\mathrm{T},\pi/2,\pi} \underline{\mathbf{h}}},$$

where

$$\mathbf{\Gamma}_{\mathrm{T},0,\pi/2} = \frac{1}{2}\int_0^{\pi/2} \underline{\mathbf{G}}\left(\cos\theta\right) \underline{\mathbf{G}}^T\left(\cos\theta\right) \sin\theta d\theta, \tag{41}$$

$$\mathbf{\Gamma}_{\mathrm{T},\pi/2,\pi} = \frac{1}{2}\int_{\pi/2}^{\pi} \underline{\mathbf{G}}\left(\cos\theta\right) \underline{\mathbf{G}}^T\left(\cos\theta\right) \sin\theta d\theta. \tag{42}$$

Mean-Squared Error

Now, let us define the error signal between the estimated and desired signals:

$$\begin{aligned} e(t) &= z(t) - \mathbf{i}_l^T \mathbf{x}\left(t - \Delta\right) \\ &= x_{\mathrm{fd}}(t) + v_{\mathrm{rn}}(t) - \mathbf{i}_l^T \mathbf{x}\left(t - \Delta\right). \end{aligned} \tag{43}$$

This error can be rewritten as

$$e(t) = e_{\mathrm{d}}(t) + e_{\mathrm{n}}(t), \tag{44}$$

where

$$\begin{aligned} e_{\mathrm{d}}(t) &= x_{\mathrm{fd}}(t) - \mathbf{i}_l^T \mathbf{x}\left(t - \Delta\right) \\ &= \left[\underline{\mathbf{G}}^T \left(\cos\theta_{\mathrm{d}}\right) \underline{\mathbf{h}} - \mathbf{i}_l\right]^T \mathbf{x}\left(t - \Delta\right) \end{aligned} \tag{45}$$

and

$$\begin{aligned} e_{\mathrm{n}}(t) &= v_{\mathrm{rn}}(t) \\ &= \underline{\mathbf{h}}^T \underline{\mathbf{v}}(t) \end{aligned} \tag{46}$$

are, respectively, the desired-signal distortion due to the beamformer and the residual noise.

Therefore, the MSE criterion is

$$\begin{aligned} J\left(\underline{\mathbf{h}}\right) &= E\left[e^2(t)\right] \\ &= \sigma_x^2 - 2\underline{\mathbf{h}}^T \underline{\mathbf{G}} \left(\cos\theta_{\mathrm{d}}\right) \mathbf{R}_{\mathbf{x}} \mathbf{i}_l + \underline{\mathbf{h}}^T \mathbf{R}_{\underline{\mathbf{y}}} \underline{\mathbf{h}} \\ &= J_{\mathrm{d}}\left(\underline{\mathbf{h}}\right) + J_{\mathrm{n}}\left(\underline{\mathbf{h}}\right), \end{aligned} \tag{47}$$

where

$$\begin{aligned} J_{\mathrm{d}}\left(\underline{\mathbf{h}}\right) &= E\left[e_{\mathrm{d}}^{2}(t)\right] \\ &= \left[\underline{\mathbf{G}}^{T}\left(\cos_{\mathrm{d}}\theta\right)\underline{\mathbf{h}} - \mathbf{i}_{l}\right]^{T}\mathbf{R}_{\mathbf{x}}\left[\underline{\mathbf{G}}^{T}\left(\cos_{\mathrm{d}}\theta\right)\underline{\mathbf{h}} - \mathbf{i}_{l}\right] \\ &= \sigma_{x}^{2}\upsilon_{\mathrm{d}}\left(\underline{\mathbf{h}}\right) \end{aligned} \tag{48}$$

and

$$\begin{aligned} J_{\mathrm{n}}\left(\underline{\mathbf{h}}\right) &= E\left[e_{\mathrm{n}}^{2}(t)\right] \\ &= \underline{\mathbf{h}}^{T}\mathbf{R}_{\underline{\mathbf{v}}}\underline{\mathbf{h}} \\ &= \frac{\sigma_{v_1}^{2}}{\xi_{\mathrm{n}}\left(\underline{\mathbf{h}}\right)}, \end{aligned} \tag{49}$$

with

$$\upsilon_{\mathrm{d}}\left(\underline{\mathbf{h}}\right) = \frac{E\left\{\left[x_{\mathrm{fd}}(t) - \mathbf{i}_l^T \mathbf{x}\left(t-\Delta\right)\right]^2\right\}}{\sigma_x^2} \tag{50}$$
$$= \frac{\left[\underline{\mathbf{G}}^T\left(\cos_{\mathrm{d}}\theta\right)\underline{\mathbf{h}} - \mathbf{i}_l\right]^T \mathbf{R}_{\mathbf{x}}\left[\underline{\mathbf{G}}^T\left(\cos_{\mathrm{d}}\theta\right)\underline{\mathbf{h}} - \mathbf{i}_l\right]}{\sigma_x^2}$$

being the desired-signal distortion index and

$$\xi_{\mathrm{n}}\left(\underline{\mathbf{h}}\right) = \frac{\sigma_{v_1}^2}{\underline{\mathbf{h}}^T \mathbf{R}_{\underline{\mathbf{v}}}\underline{\mathbf{h}}} \tag{51}$$

being the noise reduction factor.

We deduce that

$$\begin{aligned}\frac{J_{\mathrm{d}}\left(\underline{\mathbf{h}}\right)}{J_{\mathrm{n}}\left(\underline{\mathbf{h}}\right)} &= \mathrm{iSNR}\times\xi_{\mathrm{n}}\left(\underline{\mathbf{h}}\right)\times\upsilon_{\mathrm{d}}\left(\underline{\mathbf{h}}\right) \\ &= \mathrm{oSNR}\left(\underline{\mathbf{h}}\right)\times\xi_{\mathrm{d}}\left(\underline{\mathbf{h}}\right)\times\upsilon_{\mathrm{d}}\left(\underline{\mathbf{h}}\right),\end{aligned} \tag{52}$$

where

$$\xi_{\mathrm{d}}\left(\underline{\mathbf{h}}\right)=\frac{\sigma_x^2}{\underline{\mathbf{h}}^T\mathbf{R}_{\underline{\mathbf{x}}}\underline{\mathbf{h}}} \tag{53}$$

is the desired-signal reduction factor.

Fixed Beamformers

Delay-and-Sum

In this section, we show how to derive the most conventional time-domain fixed beamformers from the WNG and the DF.

The classical delay-and-sum (DS) beamformer in the time domain is derived by maximizing the WNG subject to the distortionless constraint.

This is equivalent to

$$\min_{\underline{\mathbf{h}}} \underline{\mathbf{h}}^T \underline{\mathbf{h}} \quad \text{subject to} \quad \underline{\mathbf{h}}^T \underline{\mathbf{G}} \left(\cos\theta_{\mathrm{d}}\right) = \mathbf{i}_l^T. \tag{54}$$

We easily obtain

$$\underline{\mathbf{h}}_{\mathrm{DS}} \left(\cos\theta_{\mathrm{d}}\right) = \underline{\mathbf{G}} \left(\cos\theta_{\mathrm{d}}\right) \left[\underline{\mathbf{G}}^T \left(\cos\theta_{\mathrm{d}}\right) \underline{\mathbf{G}} \left(\cos\theta_{\mathrm{d}}\right)\right]^{-1} \mathbf{i}_l. \tag{55}$$

Therefore, the WNG is

$$\mathcal{W}\left[\underline{\mathbf{h}}_{\mathrm{DS}}\left(\cos\theta_{\mathrm{d}}\right)\right]=\frac{1}{\mathbf{i}_{l}^{T}\left[\underline{\mathbf{G}}^{T}\left(\cos\theta_{\mathrm{d}}\right)\underline{\mathbf{G}}\left(\cos\theta_{\mathrm{d}}\right)\right]^{-1}\mathbf{i}_{l}}. \tag{56}$$

It can be checked that the matrix product $\mathbf{G}_{m}^{T}\left(\cos\theta_{\mathrm{d}}\right)\mathbf{G}_{m}\left(\cos\theta_{\mathrm{d}}\right)$ is a diagonal matrix whose elements are 0 or 1.

As a result, the matrix $\underline{\mathbf{G}}^{T}\left(\cos\theta_{\mathrm{d}}\right)\underline{\mathbf{G}}\left(\cos\theta_{\mathrm{d}}\right)=\sum_{m=1}^{M}\mathbf{G}_{m}^{T}\left(\cos\theta_{\mathrm{d}}\right)\mathbf{G}_{m}\left(\cos\theta_{\mathrm{d}}\right)$ is also a diagonal matrix whose main elements are between 0 and M.

We conclude that the position of the 1 in $\mathbf{i}_{l}$ must coincide with the position of the maximum element of the diagonal of $\underline{\mathbf{G}}^{T}\left(\cos\theta_{\mathrm{d}}\right)\underline{\mathbf{G}}\left(\cos\theta_{\mathrm{d}}\right)$.

In this case, we have

$$\mathcal{W}\left[\underline{\mathbf{h}}_{\mathrm{DS}}\left(\cos\theta_{\mathrm{d}}\right)\right] = M \tag{57}$$

and

$$\underline{\mathbf{h}}_{\mathrm{DS}}\left(\cos\theta_{\mathrm{d}}\right) = \underline{\mathbf{G}}\left(\cos\theta_{\mathrm{d}}\right)\frac{\mathbf{i}_l}{M}. \tag{58}$$

In the rest, it is always assumed that the position of the 1 in $\mathbf{i}_l$ is chosen such that $\mathbf{i}_l^T\left[\underline{\mathbf{G}}^T\left(\cos\theta_{\mathrm{d}}\right)\underline{\mathbf{G}}\left(\cos\theta_{\mathrm{d}}\right)\right]^{-1}\mathbf{i}_l = 1/M$.

Example 1

Consider a ULA of M sensors.

Suppose that a desired signal impinges on the ULA from the direction θ_{d}.

Assume that $f_{\mathrm{s}} = 8$ kHz, $P = 25$, and $L_h = 30$.

Figures 4–6 show broadband beampatterns, $|\mathcal{B}\left[\underline{\mathbf{h}}_{\mathrm{DS}}\left(\cos\theta_{\mathrm{d}}\right), \cos\theta\right]|$, for different source directions θ_{d} and several values of M and δ.

The main beam is in the direction of the desired signal, i.e., θ_{d}.

As the number of sensors, M, increases, or as the intersensor spacing, δ, increases, the width of the main beam decreases, and the values obtained for $\theta \neq \theta_{\mathrm{d}}$ become lower.

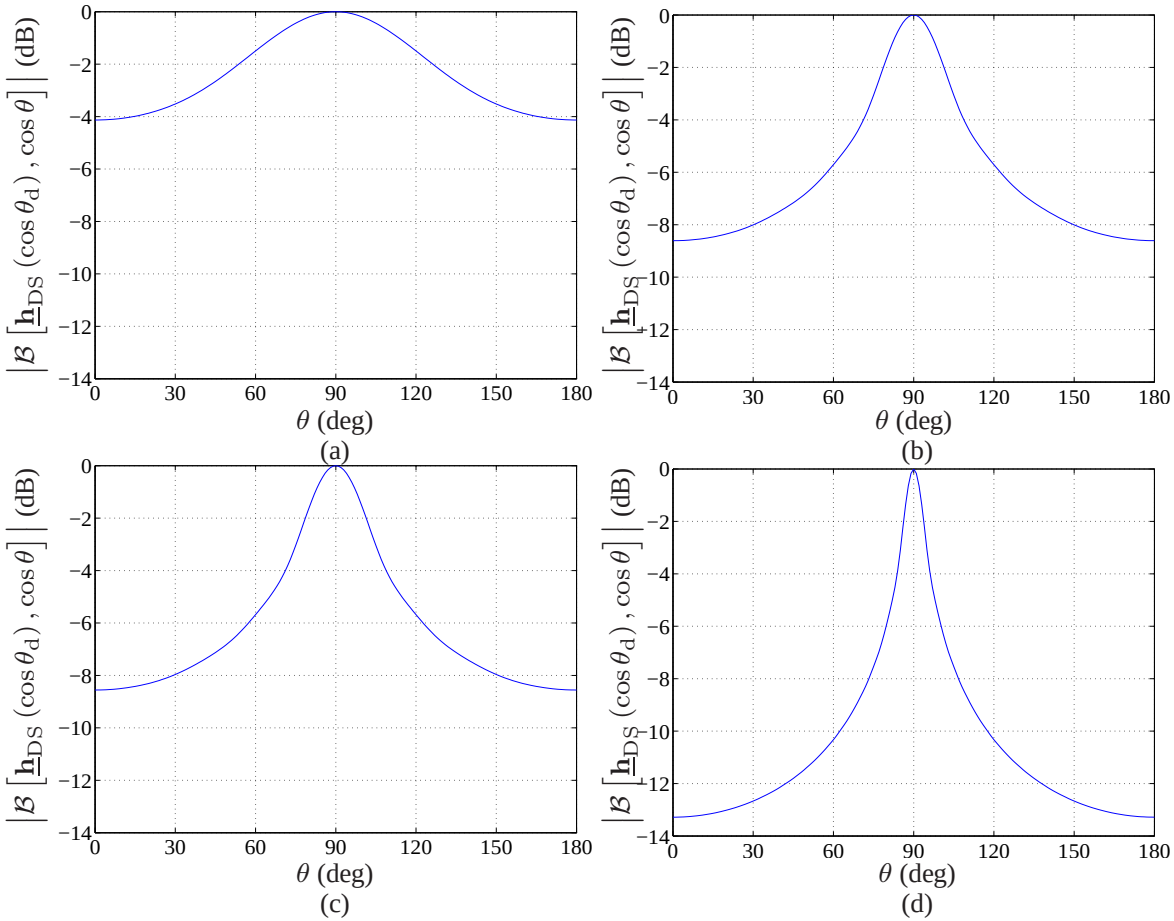

Figure 4: Broadband beampatterns of the DS beamformer for $\theta_{\mathrm{d}} = 90°$, and several values of M and δ: (a) $M = 10$, $\delta = 1$ cm, (b) $M = 30$, $\delta = 1$ cm, (c) $M = 10$, $\delta = 3$ cm, and (d) $M = 30$, $\delta = 3$ cm.

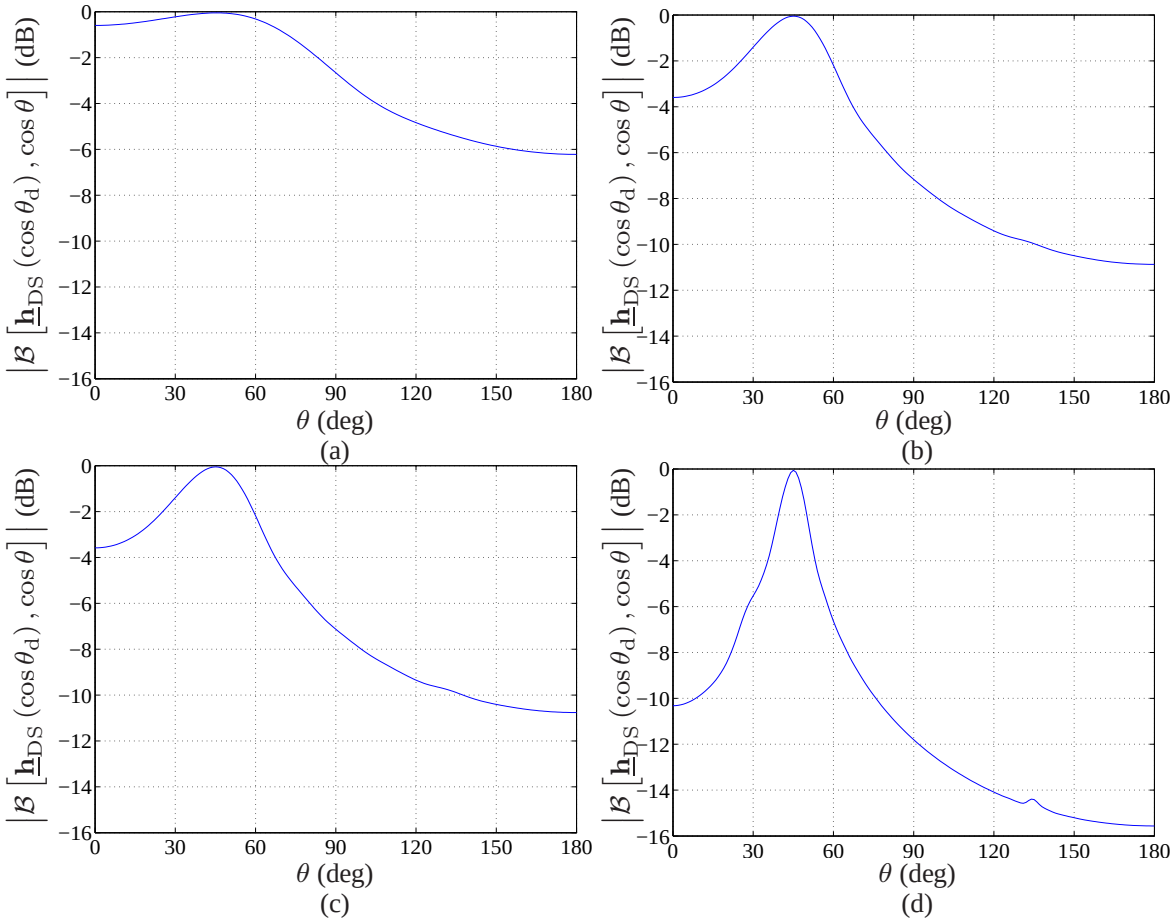

Figure 5: Broadband beampatterns of the DS beamformer for $\theta_{\mathrm{d}} = 45°$, and several values of M and δ: (a) $M = 10$, $\delta = 1$ cm, (b) $M = 30$, $\delta = 1$ cm, (c) $M = 10$, $\delta = 3$ cm, and (d) $M = 30$, $\delta = 3$ cm.

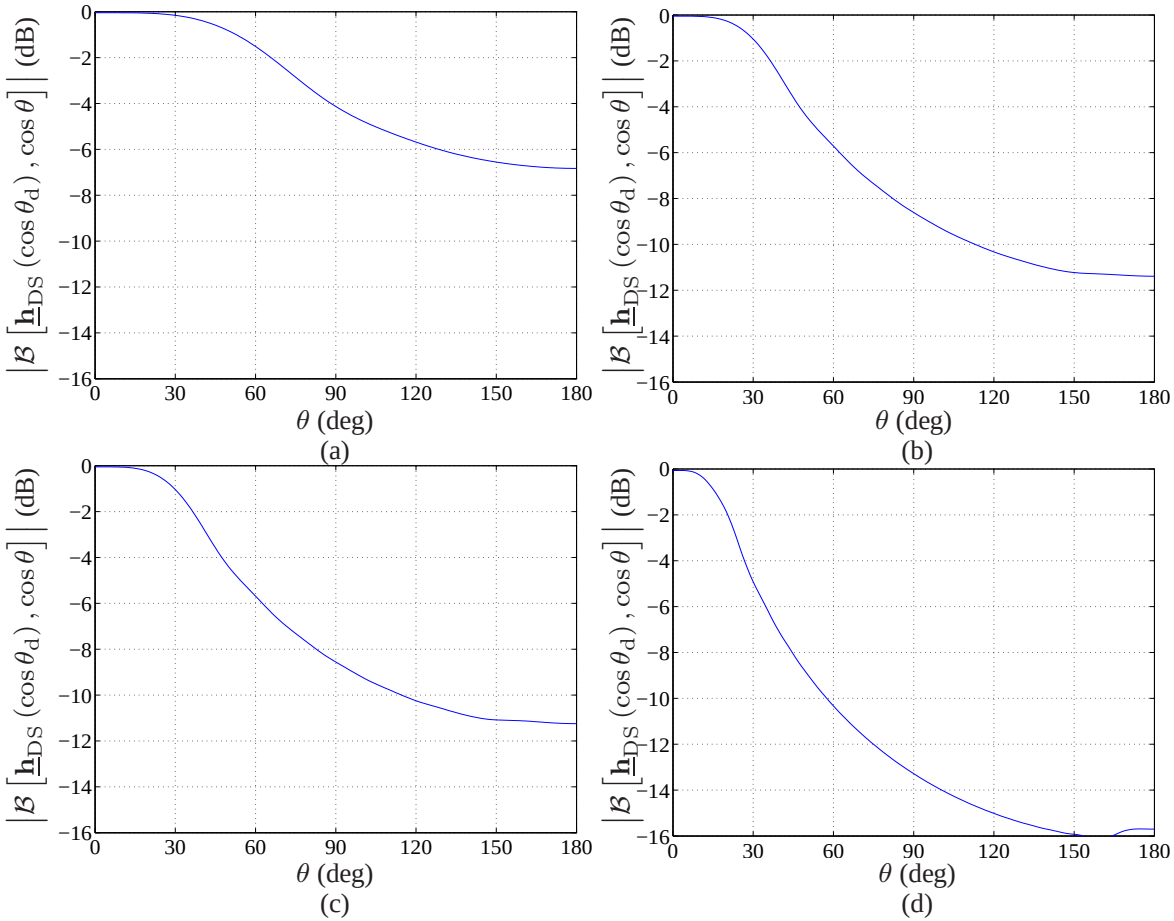

Figure 6: Broadband beampatterns of the DS beamformer for $\theta_{\mathrm{d}} = 0^\circ$, and several values of M and δ: (a) $M = 10$, $\delta = 1$ cm, (b) $M = 30$, $\delta = 1$ cm, (c) $M = 10$, $\delta = 3$ cm, and (d) $M = 30$, $\delta = 3$ cm.

Figure 7 shows plots of the DF, $\mathcal{D}\left[\underline{\mathbf{h}}_{\mathrm{DS}}\left(\cos\theta_{\mathrm{d}}\right)\right]$, and the WNG, $\mathcal{W}\left[\underline{\mathbf{h}}_{\mathrm{DS}}\left(\cos\theta_{\mathrm{d}}\right)\right]$, as a function of δ for $\theta_{\mathrm{d}}=90^{\circ}$ and several values of M.

As the number of sensors increases, both the DF and the WNG of the DS beamformer increase.

For a given M, the DF of the DS beamformer increases as a function of δ.

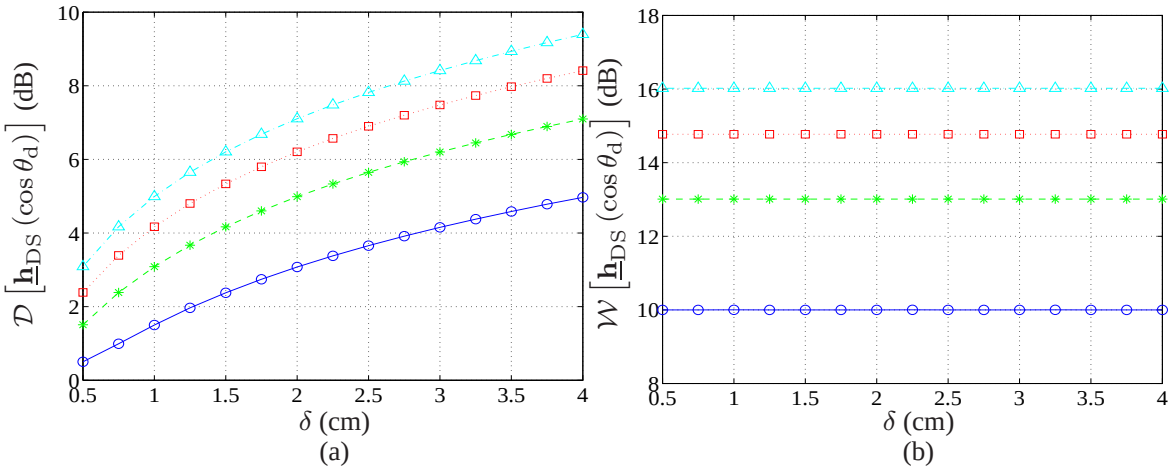

Figure 7: (a) DF and (b) WNG of the DS beamformer as a function of δ for $\theta_{\mathrm{d}} = 90°$ and several values of M: $M = 10$ (solid line with circles), $M = 20$ (dashed line with asterisks), $M = 30$ (dotted line with squares), and $M = 40$ (dash-dot line with triangles).

Maximum DF

Let $\underline{\mathbf{t}}_1\left(\cos\theta_{\mathrm{d}}\right)$ be the eigenvector corresponding to the maximum eigenvalue, $\underline{\lambda}_1\left(\cos\theta_{\mathrm{d}}\right)$, of the matrix $\mathbf{\Gamma}_{\mathrm{T},0,\pi}^{-1}\underline{\mathbf{G}}\left(\cos\theta_{\mathrm{d}}\right)\underline{\mathbf{G}}^{T}\left(\cos\theta_{\mathrm{d}}\right)$.

It is obvious that the maximum DF beamformer is

$$\underline{\mathbf{h}}_{\max}\left(\cos\theta_{\mathrm{d}}\right)=\varsigma\underline{\mathbf{t}}_1\left(\cos\theta_{\mathrm{d}}\right), \tag{59}$$

where $\varsigma\neq 0$ is an arbitrary real number, and the maximum DF is

$$\mathcal{D}_{\max}\left(\cos\theta_{\mathrm{d}}\right)=\underline{\lambda}_1\left(\cos\theta_{\mathrm{d}}\right). \tag{60}$$

Therefore,

$$\mathcal{D}_{\max}\left(\cos\theta_{\mathrm{d}}\right)\geq\mathcal{D}\left(\underline{\mathbf{h}}\right),\ \forall\underline{\mathbf{h}}. \tag{61}$$

While $\underline{\mathbf{h}}_{\max}\left(\cos\theta_{\mathrm{d}}\right)$ maximizes the DF, it cannot be distortionless.

Distortionless Maximum DF

To find the distortionless maximum DF beamformer, we need to minimize the denominator of the DF subject to the distortionless constraint in the numerator of the DF, i.e.,

$$\min_{\underline{\mathbf{h}}} \underline{\mathbf{h}}^T \mathbf{\Gamma}_{\mathrm{T},0,\pi} \underline{\mathbf{h}} \quad \text{subject to} \quad \underline{\mathbf{h}}^T \underline{\mathbf{G}} \left(\cos\theta_{\mathrm{d}}\right) = \mathbf{i}_l^T. \tag{62}$$

Then, it is clear that the distortionless maximum DF beamformer is

$$\underline{\mathbf{h}}_{\mathrm{mDF}} \left(\cos\theta_{\mathrm{d}}\right) = \mathbf{\Gamma}_{\mathrm{T},0,\pi}^{-1} \underline{\mathbf{G}} \left(\cos\theta_{\mathrm{d}}\right) \left[\underline{\mathbf{G}}^T \left(\cos\theta_{\mathrm{d}}\right) \mathbf{\Gamma}_{\mathrm{T},0,\pi}^{-1} \underline{\mathbf{G}} \left(\cos\theta_{\mathrm{d}}\right)\right]^{-1} \mathbf{i}_l. \tag{63}$$

We deduce that the corresponding DF is

$$\mathcal{D}\left[\underline{\mathbf{h}}_{\mathrm{mDF}} \left(\cos\theta_{\mathrm{d}}\right)\right] = \frac{1}{\mathbf{i}_l^T \left[\underline{\mathbf{G}}^T \left(\cos\theta_{\mathrm{d}}\right) \mathbf{\Gamma}_{\mathrm{T},0,\pi}^{-1} \underline{\mathbf{G}} \left(\cos\theta_{\mathrm{d}}\right)\right]^{-1} \mathbf{i}_l}. \tag{64}$$

Example 2

Returning to Example 1, we now employ the distortionless maximum DF beamformer, $\underline{\mathbf{h}}_{\mathrm{mDF}}\left(\cos\theta_{\mathrm{d}}\right)$, given in (63).

Figures 8–10 show broadband beampatterns, $\left|\mathcal{B}\left[\underline{\mathbf{h}}_{\mathrm{mDF}}\left(\cos\theta_{\mathrm{d}}\right),\cos\theta\right]\right|$, for different source directions θ_{d} and several values of M and δ.

The main beam is in the direction of the desired signal, i.e., θ_{d}.

As the number of sensors, M, increases, or as the intersensor spacing, δ, increases, the width of the main beam decreases, and the values obtained for $\theta \neq \theta_{\mathrm{d}}$ generally become lower.

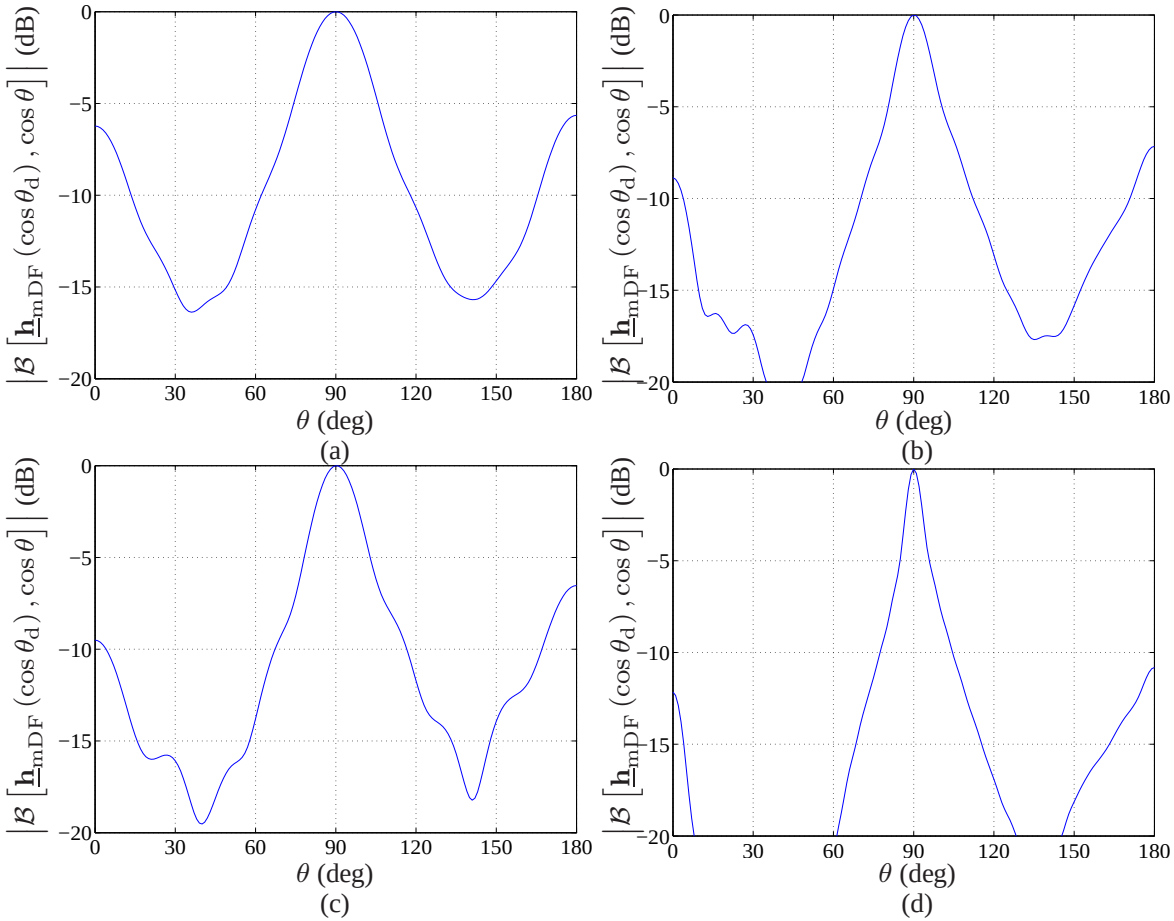

Figure 8: Broadband beampatterns of the distortionless maximum DF beamformer for $\theta_{\mathrm{d}} = 90°$, and several values of M and δ: (a) $M = 10$, $\delta = 1$ cm, (b) $M = 30$, $\delta = 1$ cm, (c) $M = 10$, $\delta = 3$ cm, and (d) $M = 30$, $\delta = 3$ cm.

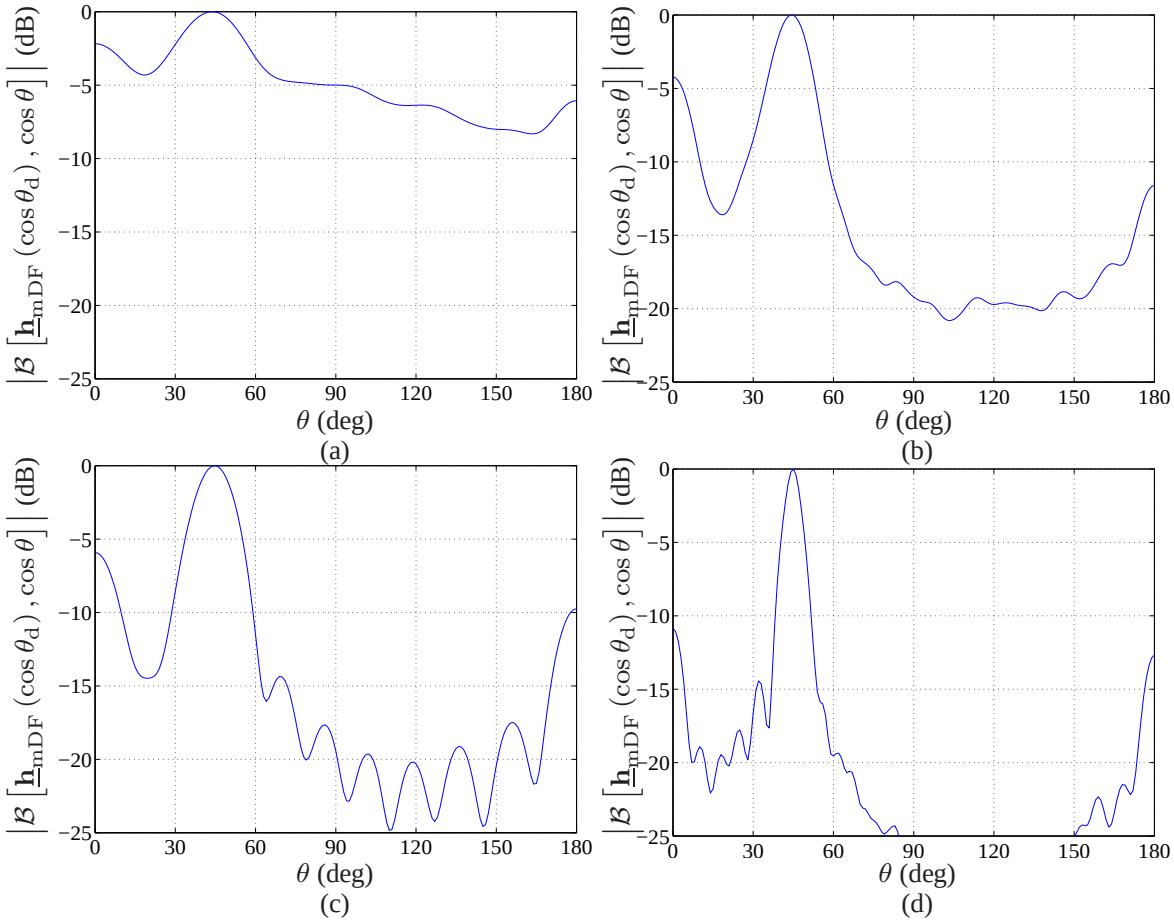

Figure 9: Broadband beampatterns of the distortionless maximum DF beamformer for $\theta_{\mathrm{d}} = 45°$, and several values of M and δ: (a) $M = 10$, $\delta = 1$ cm, (b) $M = 30$, $\delta = 1$ cm, (c) $M = 10$, $\delta = 3$ cm, and (d) $M = 30$, $\delta = 3$ cm.

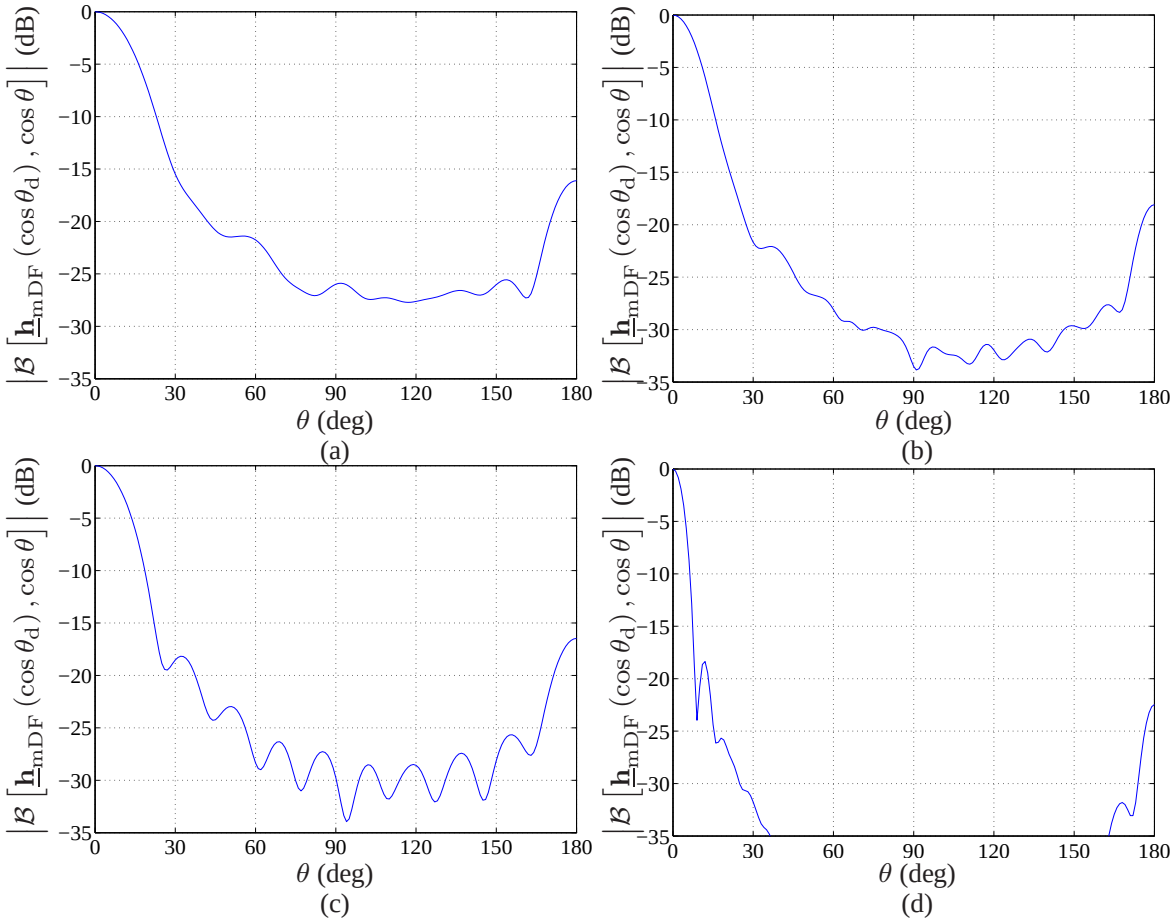

Figure 10: Broadband beampatterns of the distortionless maximum DF beamformer for $\theta_{\mathrm{d}} = 0°$, and several values of M and δ: (a) $M = 10$, $\delta = 1$ cm, (b) $M = 30$, $\delta = 1$ cm, (c) $M = 10$, $\delta = 3$ cm, and (d) $M = 30$, $\delta = 3$ cm.

Figure 11 shows plots of the DF, $\mathcal{D}\left[\underline{\mathbf{h}}_{\mathrm{mDF}}\left(\cos\theta_{\mathrm{d}}\right)\right]$, and the WNG, $\mathcal{W}\left[\underline{\mathbf{h}}_{\mathrm{mDF}}\left(\cos\theta_{\mathrm{d}}\right)\right]$, as a function of δ for $\theta_{\mathrm{d}} = 0^{\circ}$ and several values of M.

Compared to the DS beamformer, the distortionless maximum DF beamformer obtains higher DF, but lower WNG (cf. Figs. 7 and 11).

For a sufficiently small δ, as the number of sensors increases, both the DF and the WNG of the DS beamformer increase.

For a given M and a sufficiently small δ, the DF of the distortionless maximum DF beamformer increases as a function of δ.

The WNG of the distortionless maximum DF beamformer is significantly lower than 0 dB, which implies that the distortionless maximum DF beamformer amplifies the white noise.

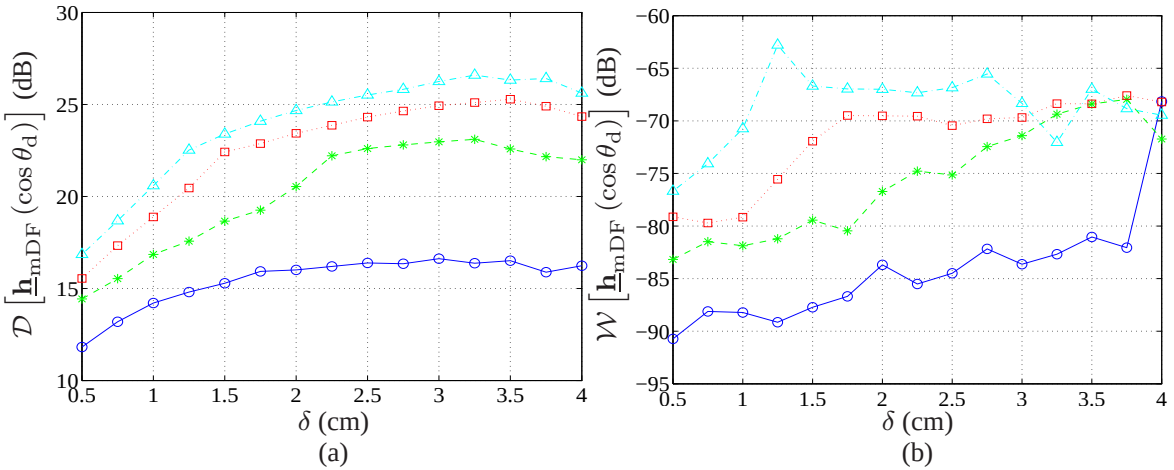

Figure 11: (a) DF and (b) WNG of the distortionless maximum DF beamformer as a function of δ for $\theta_{\mathrm{d}} = 0^\circ$ and several values of M: $M = 10$ (solid line with circles), $M = 20$ (dashed line with asterisks), $M = 30$ (dotted line with squares), and $M = 40$ (dash-dot line with triangles).

Superdirective

The time-domain superdirective beamformer is simply a particular case of the distortionless maximum DF beamformer, where $\theta_{\mathrm{d}} = 0$ and δ is small.

We get

$$\underline{\mathbf{h}}_{\mathrm{SD}} = \boldsymbol{\Gamma}_{\mathrm{T},0,\pi}^{-1}\underline{\mathbf{G}}\left(\underline{\mathbf{G}}^{T}\boldsymbol{\Gamma}_{\mathrm{T},0,\pi}^{-1}\underline{\mathbf{G}}\right)^{-1}\mathbf{i}_{l}, \tag{65}$$

where $\underline{\mathbf{G}} = \underline{\mathbf{G}}\left(\cos 0\right)$.

The corresponding DF is

$$\mathcal{D}\left(\underline{\mathbf{h}}_{\mathrm{SD}}\right) = \frac{1}{\mathbf{i}_{l}^{T}\left(\underline{\mathbf{G}}^{T}\boldsymbol{\Gamma}_{\mathrm{T},0,\pi}^{-1}\underline{\mathbf{G}}\right)^{-1}\mathbf{i}_{l}}. \tag{66}$$

This gain should approach M^2 for a small value of δ.

Following the ideas in [4], [5], we can easily derive the time-domain robust superdirective beamformer:

$$\underline{\mathbf{h}}_{\mathrm{R},\epsilon} = \mathbf{\Gamma}_{\mathrm{T},0,\pi,\epsilon}^{-1}\underline{\mathbf{G}}\left(\underline{\mathbf{G}}^{T}\mathbf{\Gamma}_{\mathrm{T},0,\pi,\epsilon}^{-1}\underline{\mathbf{G}}\right)^{-1}\mathbf{i}_{l}, \tag{67}$$

where

$$\mathbf{\Gamma}_{\mathrm{T},0,\pi,\epsilon} = \mathbf{\Gamma}_{\mathrm{T},0,\pi} + \epsilon\mathbf{I}_{ML_h}, \tag{68}$$

with $\epsilon \geq 0$.

We see that $\underline{\mathbf{h}}_{\mathrm{R},0} = \underline{\mathbf{h}}_{\mathrm{SD}}$ and $\underline{\mathbf{h}}_{\mathrm{R},\infty} = \underline{\mathbf{h}}_{\mathrm{DS}}$ (1).

Example 3

Returning to Example 1, we now employ the robust superdirective beamformer, $\underline{\mathbf{h}}_{\mathrm{R},\epsilon}$, given in (67).

Figure 12 shows broadband beampatterns, $\left|\mathcal{B}\left(\underline{\mathbf{h}}_{\mathrm{R},\epsilon}, \cos\theta\right)\right|$, for $M = 10$, $\delta = 1$ cm, and several values of ϵ.

The main beam is in the direction of the desired signal, i.e., $\theta_{\mathrm{d}} = 0$.

As the value of ϵ increases, the width of the main beam increases, and the sidelobe level also increases (lower DF).

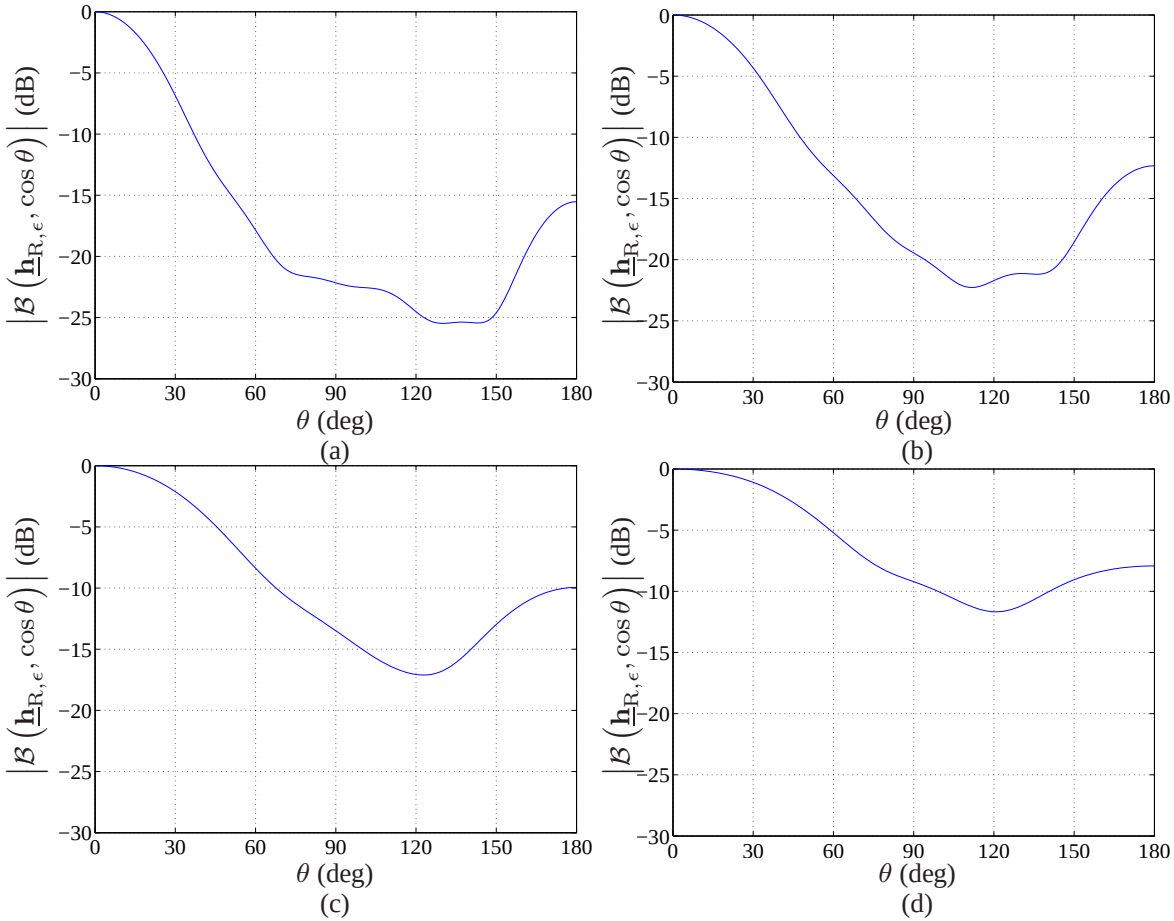

Figure 12: Broadband beampatterns of the robust superdirective beamformer for $M = 10$, $\delta = 1$ cm, and several values of ϵ: (a) $\epsilon = 10^{-5}$, (b) $\epsilon = 10^{-3}$, (c) $\epsilon = 0.1$, and (d) $\epsilon = 1$.

Figure 13 shows plots of the DF, $\mathcal{D}\left(\underline{\mathbf{h}}_{\mathrm{R},\epsilon}\right)$, and the WNG, $\mathcal{W}\left(\underline{\mathbf{h}}_{\mathrm{R},\epsilon}\right)$, as a function of δ for several values of ϵ.

For a given δ, as the value of ϵ increases, the WNG of the robust superdirective beamformer increases at the expense of a lower DF.

For a given ϵ and a sufficiently small δ, both the DF and the WNG of the robust superdirective beamformer increase as a function of δ.

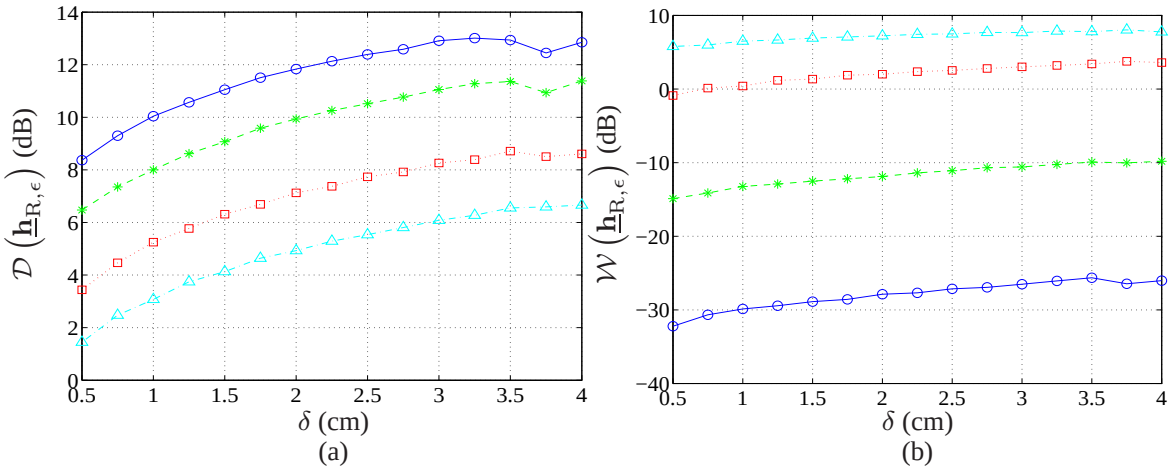

Figure 13: (a) DF and (b) WNG of the robust superdirective beamformer as a function of δ for $M = 10$ and several values of ϵ: $\epsilon = 10^{-5}$ (solid line with circles), $\epsilon = 10^{-3}$ (dashed line with asterisks), $\epsilon = 0.1$ (dotted line with squares), and $\epsilon = 1$ (dash-dot line with triangles).

Null Steering

We assume that we have an undesired source impinging on the array from the direction $\theta_{\mathrm{n}} \neq \theta_{\mathrm{d}}$.

The objective is to completely cancel this source while recovering the desired source impinging on the array from the direction θ_{d}.

Then, it is obvious that the constraint equation is

$$\underline{\mathbf{C}}^{T}\left(\theta_{\mathrm{d}}, \theta_{\mathrm{n}}\right) \underline{\mathbf{h}} = \begin{bmatrix} \mathbf{i}_{l} \\ \mathbf{0} \end{bmatrix}, \tag{69}$$

where

$$\underline{\mathbf{C}}\left(\theta_{\mathrm{d}}, \theta_{\mathrm{n}}\right) = \begin{bmatrix} \underline{\mathbf{G}}\left(\cos\theta_{\mathrm{d}}\right) & \underline{\mathbf{G}}\left(\cos\theta_{\mathrm{n}}\right) \end{bmatrix} \tag{70}$$

is the constraint matrix of size $ML_h \times 2L$ and $\mathbf{0}$ is the zero vector of length L.

Depending on what we desire, there are different ways to achieve the goal explained above.

Next, we present two methods.

The first obvious beamformer is obtained by maximizing the WNG and by taking (69) into account, i.e.,

$$\min_{\underline{\mathbf{h}}} \underline{\mathbf{h}}^T \underline{\mathbf{h}} \quad \text{subject to} \quad \underline{\mathbf{C}}^T (\theta_{\mathrm{d}}, \theta_{\mathrm{n}}) \underline{\mathbf{h}} = \begin{bmatrix} \mathbf{i}_l \\ \mathbf{0} \end{bmatrix}. \tag{71}$$

From this criterion, we find the minimum-norm (MN) beamformer:

$$\underline{\mathbf{h}}_{\mathrm{MN}} (\cos\theta_{\mathrm{d}}) = \underline{\mathbf{C}} (\theta_{\mathrm{d}}, \theta_{\mathrm{n}}) \left[\underline{\mathbf{C}}^T (\theta_{\mathrm{d}}, \theta_{\mathrm{n}}) \underline{\mathbf{C}} (\theta_{\mathrm{d}}, \theta_{\mathrm{n}}) \right]^{-1} \begin{bmatrix} \mathbf{i}_l \\ \mathbf{0} \end{bmatrix}, \tag{72}$$

which is also the minimum-norm solution of (69).

The other beamformer is obtained by maximizing the DF and by taking (69) into account, i.e.,

$$\min_{\underline{\mathbf{h}}} \underline{\mathbf{h}}^T \mathbf{\Gamma}_{\mathrm{T},0,\pi} \underline{\mathbf{h}} \quad \text{subject to} \quad \underline{\mathbf{C}}^T (\theta_{\mathrm{d}}, \theta_{\mathrm{n}}) \underline{\mathbf{h}} = \begin{bmatrix} \mathbf{i}_l \\ \mathbf{0} \end{bmatrix}. \tag{73}$$

We easily find the null steering (NS) beamformer:

$$\underline{\mathbf{h}}_{\mathrm{NS}} (\cos\theta_{\mathrm{d}}) = \mathbf{\Gamma}^{-1}_{\mathrm{T},0,\pi} \underline{\mathbf{C}} (\theta_{\mathrm{d}}, \theta_{\mathrm{n}}) \times \left[\underline{\mathbf{C}}^T (\theta_{\mathrm{d}}, \theta_{\mathrm{n}}) \mathbf{\Gamma}^{-1}_{\mathrm{T},0,\pi} \underline{\mathbf{C}} (\theta_{\mathrm{d}}, \theta_{\mathrm{n}}) \right]^{-1} \begin{bmatrix} \mathbf{i}_l \\ \mathbf{0} \end{bmatrix}. \tag{74}$$

Example 4

Consider a ULA of M sensors.

Suppose that a desired signal impinges on the ULA from the direction $\theta_{\mathrm{d}} = 0^{\circ}$, and an undesired interference impinges on the ULA from the direction $\theta_{\mathrm{n}} = 90^{\circ}$.

Assume that $f_{\mathrm{s}} = 8$ kHz, $P = 25$, and $L_h = 30$.

Figure 14 shows broadband beampatterns, $|\mathcal{B}\left[\underline{\mathbf{h}}_{\mathrm{MN}}\left(\cos\theta_{\mathrm{d}}\right), \cos\theta\right]|$, for several values of M and δ.

Clearly, the beam is in the direction of the desired signal, i.e., θ_{d}, and the null is in the direction of the interfering signal, i.e., θ_{n}.

As the number of sensors, M, increases, or as the intersensor spacing, δ, increases, the width of the main beam and the level of the sidelobe decrease.

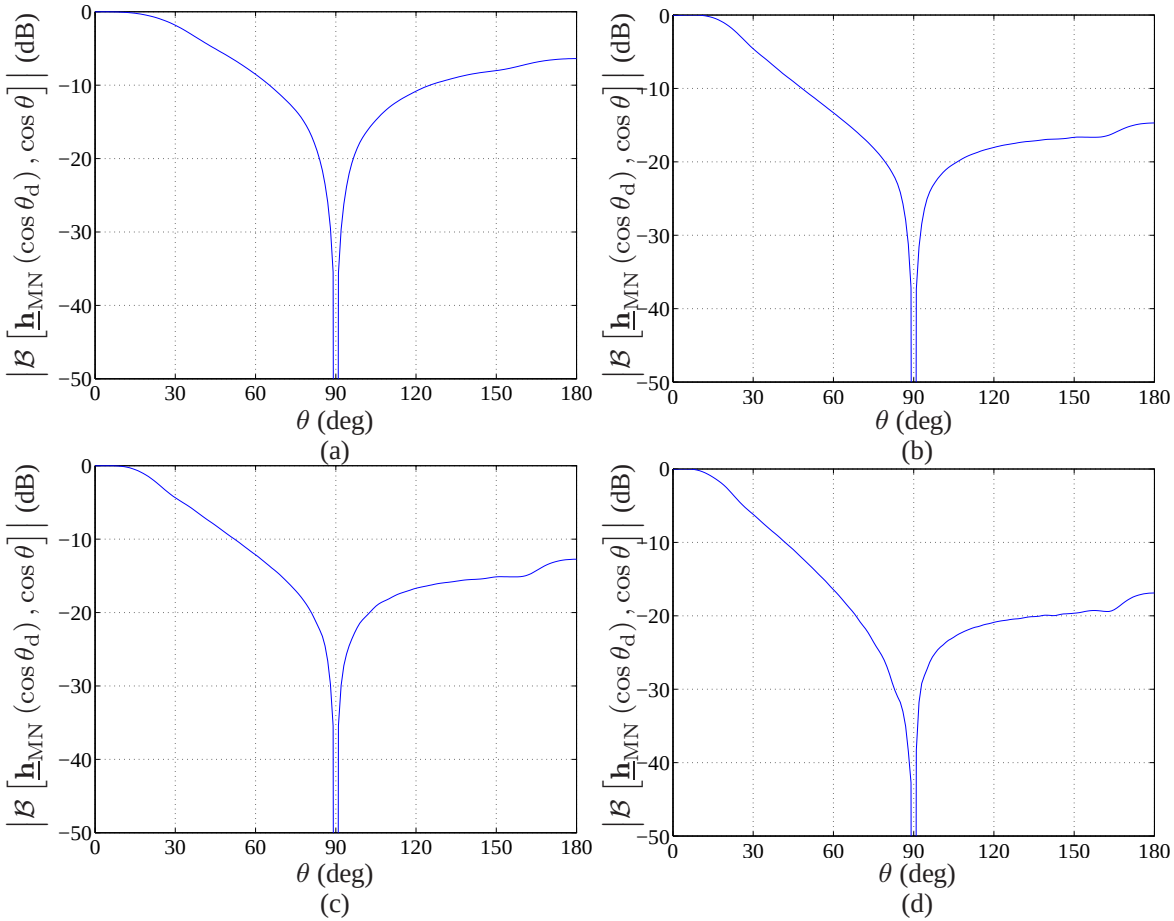

Figure 14: Broadband beampatterns of the MN beamformer for $\theta_{\mathrm{d}} = 0°$, $\theta_{\mathrm{n}} = 90°$, and several values of M and δ: (a) $M = 20$, $\delta = 2$ cm, (b) $M = 40$, $\delta = 2$ cm, (c) $M = 20$, $\delta = 4$ cm, and (d) $M = 40$, $\delta = 4$ cm.

Figure 15 shows plots of the DF, $\mathcal{D}\left[\underline{\mathbf{h}}_{\mathrm{MN}}\left(\cos\theta_{\mathrm{d}}\right)\right]$, and the WNG, $\mathcal{W}\left[\underline{\mathbf{h}}_{\mathrm{MN}}\left(\cos\theta_{\mathrm{d}}\right)\right]$, as a function of δ for several values of M.

For a small δ, both the DF and the WNG increase as M increases.

However, for a large δ, the DF and the WNG of the MN beamformer are less sensitive to M, if M is sufficiently large.

For a given M and small δ, both the DF and the WNG of the MN beamformer increase as a function of δ.

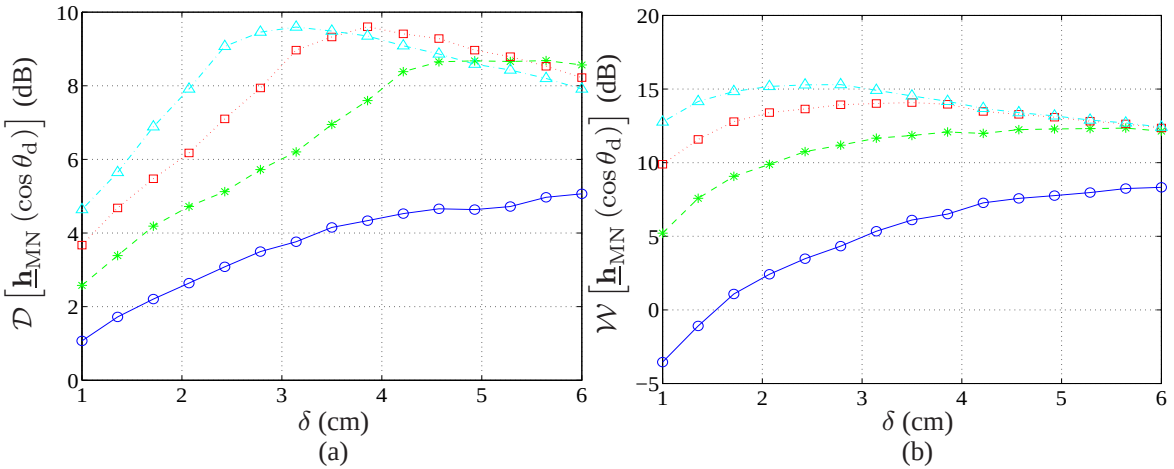

Figure 15: (a) DF and (b) WNG of the MN beamformer as a function of δ, for $\theta_{\mathrm{d}} = 0°$, $\theta_{\mathrm{n}} = 90°$, and several values of M: $M = 10$ (solid line with circles), $M = 20$ (dashed line with asterisks), $M = 30$ (dotted line with squares), and $M = 40$ (dash-dot line with triangles).

Figure 16 shows broadband beampatterns, $|\mathcal{B}\left[\underline{\mathbf{h}}_{\mathrm{NS}}\left(\cos\theta_{\mathrm{d}}\right),\cos\theta\right]|$, for several values of M and δ.

Here again, the beam is in the direction of the desired signal, and the null is in the direction of the interfering signal.

As the number of sensors, M, increases, or as the intersensor spacing, δ, increases, the width of the main beam and the level of the sidelobe decrease.

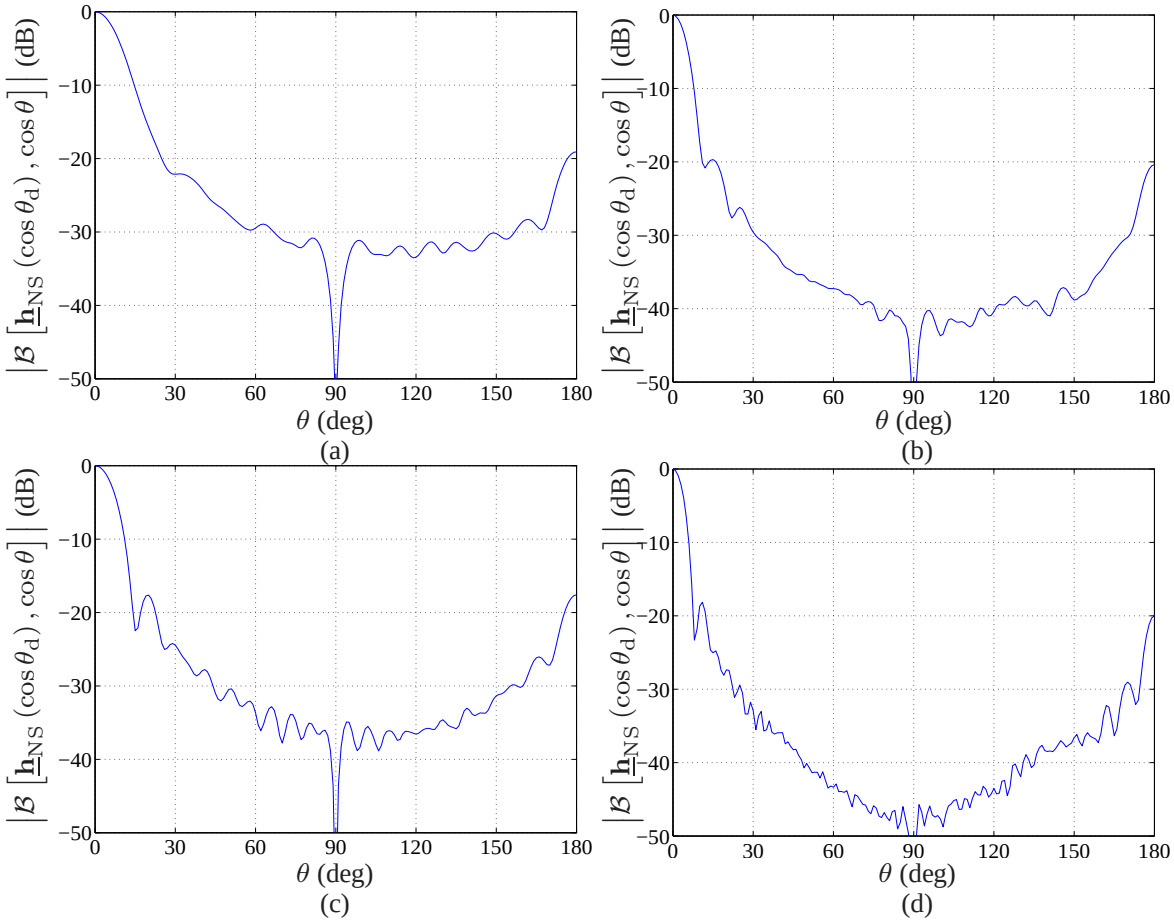

Figure 16: Broadband beampatterns of the NS beamformer for $\theta_{\mathrm{d}} = 0°$, $\theta_{\mathrm{n}} = 90°$, and several values of M and δ: (a) $M = 20$, $\delta = 2$ cm, (b) $M = 40$, $\delta = 2$ cm, (c) $M = 20$, $\delta = 4$ cm, and (d) $M = 40$, $\delta = 4$ cm.

Figure 17 shows plots of the DF, $\mathcal{D}\left[\underline{\mathbf{h}}_{\mathrm{NS}}\left(\cos\theta_{\mathrm{d}}\right)\right]$, and the WNG, $\mathcal{W}\left[\underline{\mathbf{h}}_{\mathrm{NS}}\left(\cos\theta_{\mathrm{d}}\right)\right]$, as a function of δ for several values of M.

For a small δ, both the DF and the WNG of the NS beamformer increase as M increases.

For a given M and small δ, the DF of the NS beamformer increases as a function of δ.

Compared with the MN beamformer, the NS beamformer obtains higher DF, but lower WNG.

The WNG of the NS beamformer is significantly lower than 0 dB, which implies that the NS beamformer amplifies the white noise.

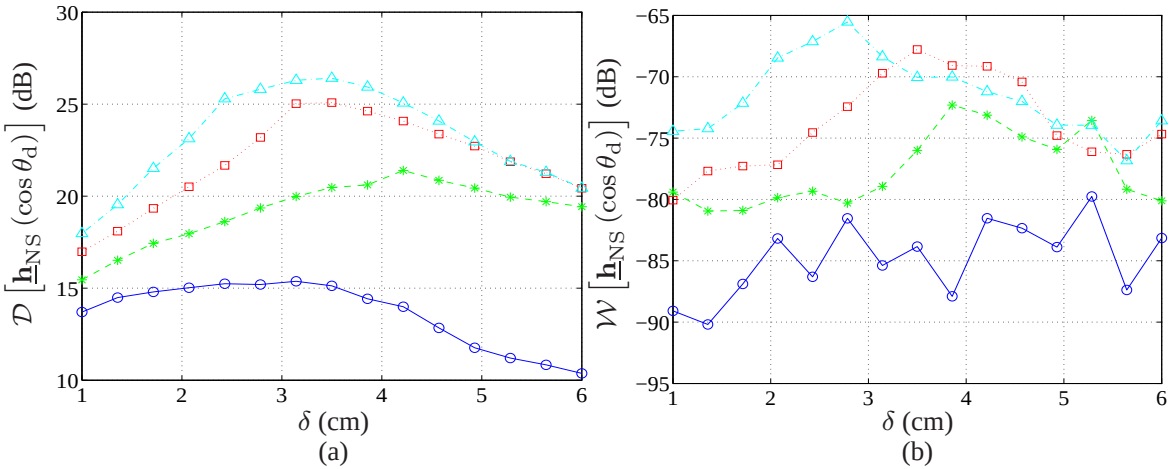

Figure 17: (a) DF and (b) WNG of the NS beamformer as a function of δ, for $\theta_{\mathrm{d}} = 0°$, $\theta_{\mathrm{n}} = 90°$, and several values of M: $M = 10$ (solid line with circles), $M = 20$ (dashed line with asterisks), $M = 30$ (dotted line with squares), and $M = 40$ (dash-dot line with triangles).

In Table 1, we summarize all the time-domain fixed beamformers derived in this section.

Table 1: Fixed beamformers in the time domain.

DS:	$\underline{\mathbf{h}}_{\mathrm{DS}}\left(\cos\theta_{\mathrm{d}}\right)=\underline{\mathbf{G}}\left(\cos\theta_{\mathrm{d}}\right)\frac{\mathbf{i}_l}{M}$
Max. DF:	$\underline{\mathbf{h}}_{\max}\left(\cos\theta_{\mathrm{d}}\right)=\varsigma\underline{\mathbf{t}}_1\left(\cos\theta_{\mathrm{d}}\right),\ \varsigma\neq 0$
Dist. Max. DF:	$\underline{\mathbf{h}}_{\mathrm{mDF}}\left(\cos\theta_{\mathrm{d}}\right)=\mathbf{\Gamma}_{\mathrm{T},0,\pi}^{-1}\underline{\mathbf{G}}\left(\cos\theta_{\mathrm{d}}\right)\times\left[\underline{\mathbf{G}}^{T}\left(\cos\theta_{\mathrm{d}}\right)\mathbf{\Gamma}_{\mathrm{T},0,\pi}^{-1}\underline{\mathbf{G}}\left(\cos\theta_{\mathrm{d}}\right)\right]^{-1}\mathbf{i}_l$
Superdirective:	$\underline{\mathbf{h}}_{\mathrm{SD}}=\mathbf{\Gamma}_{\mathrm{T},0,\pi}^{-1}\underline{\mathbf{G}}\left(\underline{\mathbf{G}}^{T}\mathbf{\Gamma}_{\mathrm{T},0,\pi}^{-1}\underline{\mathbf{G}}\right)^{-1}\mathbf{i}_l$
Robust SD:	$\underline{\mathbf{h}}_{\mathrm{R},\epsilon}=\mathbf{\Gamma}_{\mathrm{T},0,\pi,\epsilon}^{-1}\underline{\mathbf{G}}\left(\underline{\mathbf{G}}^{T}\mathbf{\Gamma}_{\mathrm{T},0,\pi,\epsilon}^{-1}\underline{\mathbf{G}}\right)^{-1}\mathbf{i}_l$
Minimum Norm:	$\underline{\mathbf{h}}_{\mathrm{MN}}\left(\cos\theta_{\mathrm{d}}\right)=\underline{\mathbf{C}}\left(\theta_{\mathrm{d}},\theta_{\mathrm{n}}\right)\left[\underline{\mathbf{C}}^{T}\left(\theta_{\mathrm{d}},\theta_{\mathrm{n}}\right)\underline{\mathbf{C}}\left(\theta_{\mathrm{d}},\theta_{\mathrm{n}}\right)\right]^{-1}\begin{bmatrix}\mathbf{i}_l\\ \mathbf{0}\end{bmatrix}$
Null Steering:	$\underline{\mathbf{h}}_{\mathrm{NS}}\left(\cos\theta_{\mathrm{d}}\right)=\mathbf{\Gamma}_{\mathrm{T},0,\pi}^{-1}\underline{\mathbf{C}}\left(\theta_{\mathrm{d}},\theta_{\mathrm{n}}\right)\times\left[\underline{\mathbf{C}}^{T}\left(\theta_{\mathrm{d}},\theta_{\mathrm{n}}\right)\mathbf{\Gamma}_{\mathrm{T},0,\pi}^{-1}\underline{\mathbf{C}}\left(\theta_{\mathrm{d}},\theta_{\mathrm{n}}\right)\right]^{-1}\begin{bmatrix}\mathbf{i}_l\\ \mathbf{0}\end{bmatrix}$

Adaptive Beamformers

Wiener

Most of the adaptive beamformers are easily derived from the time-domain MSE criterion defined in (47).

Below, we give some important examples.

From the minimization of the MSE criterion, $J\left(\underline{\mathbf{h}}\right)$, we find the Wiener beamformer:

$$\begin{aligned}\underline{\mathbf{h}}_{\mathrm{W}}\left(\cos\theta_{\mathrm{d}}\right) &= \mathbf{R}_{\underline{\mathbf{y}}}^{-1}\underline{\mathbf{G}}\left(\cos\theta_{\mathrm{d}}\right)\mathbf{R}_{\mathbf{x}}\mathbf{i}_{l} \\ &= \mathbf{R}_{\underline{\mathbf{y}}}^{-1}\underline{\mathbf{G}}\left(\cos\theta_{\mathrm{d}}\right)\mathbf{R}_{\mathbf{x}}\underline{\mathbf{G}}^{T}\left(\cos\theta_{\mathrm{d}}\right)\underline{\mathbf{i}} \\ &= \mathbf{R}_{\underline{\mathbf{y}}}^{-1}\mathbf{R}_{\underline{\mathbf{x}}\underline{\mathbf{i}}},\end{aligned} \tag{75}$$

where $\underline{\mathbf{i}}$ is a vector of length ML_h whose all elements are 0 except for one entry which is equal to 1 in the appropriate position.

This Wiener beamformer can be rewritten as

$$\underline{\mathbf{h}}_{\mathrm{W}}\left(\cos\theta_{\mathrm{d}}\right)=\left(\mathbf{I}_{ML_h}-\mathbf{R}_{\underline{\mathbf{y}}}^{-1}\mathbf{R}_{\underline{\mathbf{v}}}\right)\underline{\mathbf{i}}. \tag{76}$$

The previous expression depends on the statistics of the observations and noise.

Determining the inverse of $\mathbf{R}_{\underline{\mathbf{y}}}$ from (16) with the Woodbury's identity, we get

$$\begin{aligned}\mathbf{R}_{\underline{\mathbf{y}}}^{-1}=\mathbf{R}_{\underline{\mathbf{v}}}^{-1}-\mathbf{R}_{\underline{\mathbf{v}}}^{-1}\underline{\mathbf{G}}\left(\cos\theta_{\mathrm{d}}\right)\times\\ \left[\mathbf{R}_{\mathbf{x}}^{-1}+\underline{\mathbf{G}}^{T}\left(\cos\theta_{\mathrm{d}}\right)\mathbf{R}_{\underline{\mathbf{v}}}^{-1}\underline{\mathbf{G}}\left(\cos\theta_{\mathrm{d}}\right)\right]^{-1}\underline{\mathbf{G}}^{T}\left(\cos\theta_{\mathrm{d}}\right)\mathbf{R}_{\underline{\mathbf{v}}}^{-1}.\end{aligned} \tag{77}$$

Substituting (77) into (75), leads to another interesting formulation of the Wiener beamformer:

$$\underline{\mathbf{h}}_{\mathrm{W}}\left(\cos\theta_{\mathrm{d}}\right)=\mathbf{R}_{\underline{\mathbf{v}}}^{-1}\underline{\mathbf{G}}\left(\cos\theta_{\mathrm{d}}\right)\times \left[\mathbf{R}_{\mathbf{x}}^{-1}+\underline{\mathbf{G}}^{T}\left(\cos\theta_{\mathrm{d}}\right)\mathbf{R}_{\underline{\mathbf{v}}}^{-1}\underline{\mathbf{G}}\left(\cos\theta_{\mathrm{d}}\right)\right]^{-1}\mathbf{i}_{l}. \quad (78)$$

The output SNR with the Wiener beamformer is greater than the input SNR but the estimated desired signal is distorted.

This distortion is supposed to decrease when the number of sensors increases.

Example 5

Consider a ULA of M sensors.

Suppose that a desired signal, $x(t)$, with the autocorrelation sequence:

$$E\left[x(t)x(t')\right] = \alpha^{|t-t'|},\ -1 < \alpha < 1$$

impinges on the ULA from the direction $\theta_{\mathrm{d}} = 0°$.

Assume that an undesired white Gaussian noise interference, $u(t)$, impinges on the ULA from the direction $\theta_{\mathrm{n}} = 90°$, i.e., $u(t) \sim \mathcal{N}\left(0, \sigma_u^2\right)$, uncorrelated with $x(t)$.

In addition, the sensors contain thermal white Gaussian noise, $w_m(t) \sim \mathcal{N}\left(0, \sigma_w^2\right)$, that are mutually uncorrelated.

The noisy received signals are given by
$y_m(t) = x_m(t) + v_m(t),\ m = 1, \ldots, M$, where
$v_m(t) = u_m(t) + w_m(t),\ m = 1, \ldots, M$ are the interference-plus-noise signals.

The elements of the $L \times L$ matrix $\mathbf{R_x}$ are

$$[\mathbf{R_x}]_{i,j} = \alpha^{|i-j|},\ i, j = 1, \ldots, L.$$

The $ML_h \times ML_h$ correlation matrix of $\underline{\mathbf{x}}(t)$ is

$$\mathbf{R}_{\underline{\mathbf{x}}} = \underline{\mathbf{G}}\left(\cos\theta_{\mathrm{d}}\right)\mathbf{R_x}\underline{\mathbf{G}}^T\left(\cos\theta_{\mathrm{d}}\right).$$

Since the interference is at the broadside direction, the $ML_h \times ML_h$ correlation matrix of $\underline{\mathbf{v}}(t)$ is

$$\mathbf{R}_{\underline{\mathbf{v}}} = \mathbf{1}_M \otimes \sigma_u^2\mathbf{I}_{L_h} + \sigma_w^2\mathbf{I}_{ML_h},$$

where $\otimes$ is the Kronecker product and $\mathbf{1}_M$ is an $M \times M$ matrix of all ones.

To demonstrate the performance of the Wiener beamformer, we choose $f_{\mathrm{s}} = 8$ kHz, $\delta = 3$ cm, $\alpha = 0.8$, $\sigma_w^2 = 0.1\sigma_u^2$, $P = 20$, and $L_h = 30$.

Figure 18 shows plots of the array gain, $\mathcal{G}\left[\underline{\mathbf{h}}_{\mathrm{W}}\left(\cos\theta_{\mathrm{d}}\right)\right]$, the noise reduction factor, $\xi_{\mathrm{n}}\left[\underline{\mathbf{h}}_{\mathrm{W}}\left(\cos\theta_{\mathrm{d}}\right)\right]$, the desired-signal reduction factor, $\xi_{\mathrm{d}}\left[\underline{\mathbf{h}}_{\mathrm{W}}\left(\cos\theta_{\mathrm{d}}\right)\right]$, and the desired-signal distortion index, $\upsilon_{\mathrm{d}}\left[\underline{\mathbf{h}}_{\mathrm{W}}\left(\cos\theta_{\mathrm{d}}\right)\right]$, as a function of the input SNR, for different numbers of sensors, M.

For a given input SNR, as the number of sensors increases, the array gain and the noise reduction factor increase, while the desired-signal reduction factor and the desired-signal distortion index decrease.

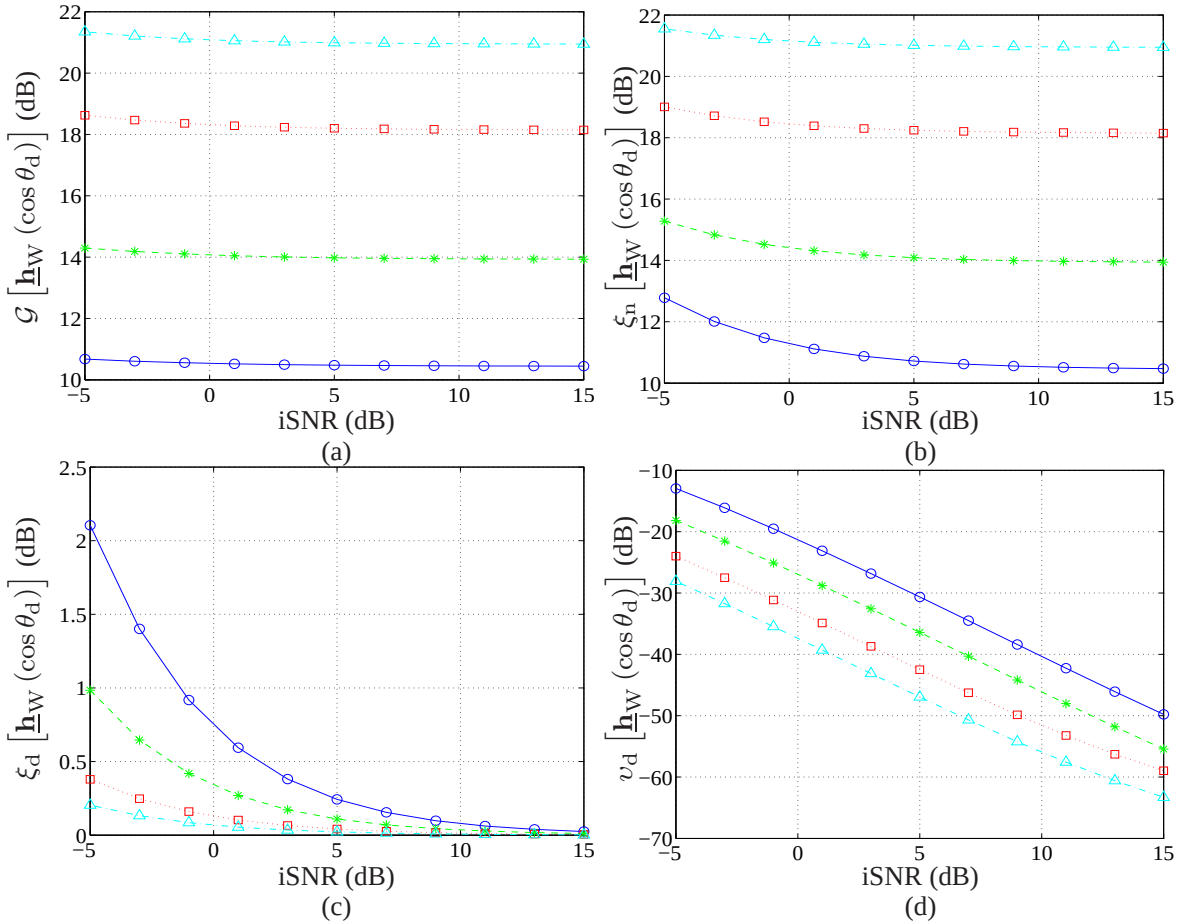

Figure 18: (a) The array gain, (b) the noise reduction factor, (c) the desired-signal reduction factor, and (d) the desired-signal distortion index of the Wiener beamformer for: $M = 4$ (solid line with circles), $M = 6$ (dashed line with asterisks), $M = 10$ (dotted line with squares), and $M = 15$ (dash-dot line with triangles).

Figure 19 shows broadband beampatterns, $|\mathcal{B}\left[\underline{\mathbf{h}}_{\mathrm{W}}\left(\cos\theta_{\mathrm{d}}\right),\cos\theta\right]|$, for different numbers of sensors, M.

The main beam is in the direction of the desired signal, i.e., θ_{d}, and there is a null in the direction of the interference, i.e., θ_{n}.

As the number of sensors increases, the width of the main beam decreases, and the null in the direction of the interference becomes deeper.

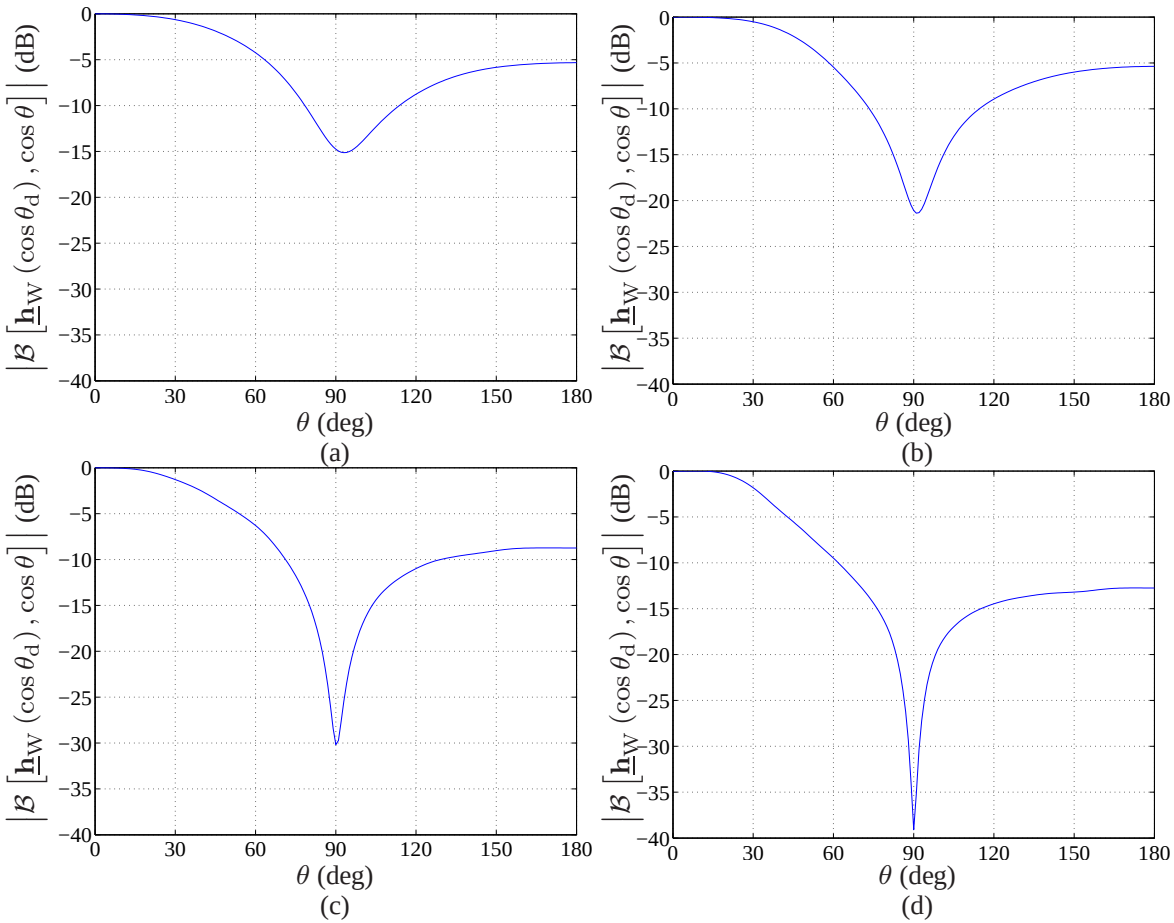

Figure 19: Broadband beampatterns of the Wiener beamformer for different numbers of sensors, M: (a) $M = 4$, (b) $M = 6$, (c) $M = 10$, and (d) $M = 15$.

MVDR

From the optimization of the criterion:

$$\min_{\underline{\mathbf{h}}} \underline{\mathbf{h}}^T \mathbf{R}_{\underline{\mathbf{v}}} \underline{\mathbf{h}} \quad \text{subject to} \quad \underline{\mathbf{h}}^T \underline{\mathbf{G}} \left(\cos\theta_{\mathrm{d}}\right) = \mathbf{i}_l^T, \tag{79}$$

we find the MVDR beamformer:

$$\underline{\mathbf{h}}_{\mathrm{MVDR}} \left(\cos\theta_{\mathrm{d}}\right) = \mathbf{R}_{\underline{\mathbf{v}}}^{-1} \underline{\mathbf{G}} \left(\cos\theta_{\mathrm{d}}\right) \left[\underline{\mathbf{G}}^T \left(\cos\theta_{\mathrm{d}}\right) \mathbf{R}_{\underline{\mathbf{v}}}^{-1} \underline{\mathbf{G}} \left(\cos\theta_{\mathrm{d}}\right)\right]^{-1} \mathbf{i}_l. \tag{80}$$

It can be shown that the MVDR beamformer is also

$$\underline{\mathbf{h}}_{\mathrm{MVDR}} \left(\cos\theta_{\mathrm{d}}\right) = \mathbf{R}_{\underline{\mathbf{y}}}^{-1} \underline{\mathbf{G}} \left(\cos\theta_{\mathrm{d}}\right) \left[\underline{\mathbf{G}}^T \left(\cos\theta_{\mathrm{d}}\right) \mathbf{R}_{\underline{\mathbf{y}}}^{-1} \underline{\mathbf{G}} \left(\cos\theta_{\mathrm{d}}\right)\right]^{-1} \mathbf{i}_l. \tag{81}$$

This formulation is more interesting in practice as it depends on the statistics of the observations only.

We always have

$$\mathrm{oSNR}\left[\underline{\mathbf{h}}_{\mathrm{MVDR}}\left(\cos\theta_{\mathrm{d}}\right)\right] \leq \mathrm{oSNR}\left[\underline{\mathbf{h}}_{\mathrm{W}}\left(\cos\theta_{\mathrm{d}}\right)\right]. \tag{82}$$

Also, with the signal model given in (1), the MVDR beamformer does not distort the desired signal.

However, in practice, since this model does not include reverberation, $\underline{\mathbf{h}}_{\mathrm{MVDR}}\left(\cos\theta_{\mathrm{d}}\right)$ may no longer be distortionless.

Example 6

Returning to Example 5, we now employ the MVDR beamformer, $\underline{\mathbf{h}}_{\mathrm{MVDR}}(\cos\theta_{\mathrm{d}})$, given in (81).

Figure 20 shows plots of the array gain, $\mathcal{G}[\underline{\mathbf{h}}_{\mathrm{MVDR}}(\cos\theta_{\mathrm{d}})]$, the noise reduction factor, $\xi_{\mathrm{n}}[\underline{\mathbf{h}}_{\mathrm{MVDR}}(\cos\theta_{\mathrm{d}})]$, the desired-signal reduction factor, $\xi_{\mathrm{d}}[\underline{\mathbf{h}}_{\mathrm{MVDR}}(\cos\theta_{\mathrm{d}})]$, and the MSE, $J[\underline{\mathbf{h}}_{\mathrm{MVDR}}(\cos\theta_{\mathrm{d}})]$, as a function of the input SNR, for different numbers of sensors, M.

For a given input SNR, as the number of sensors increases, the array gain and the noise reduction factor increase, while the MSE decreases.

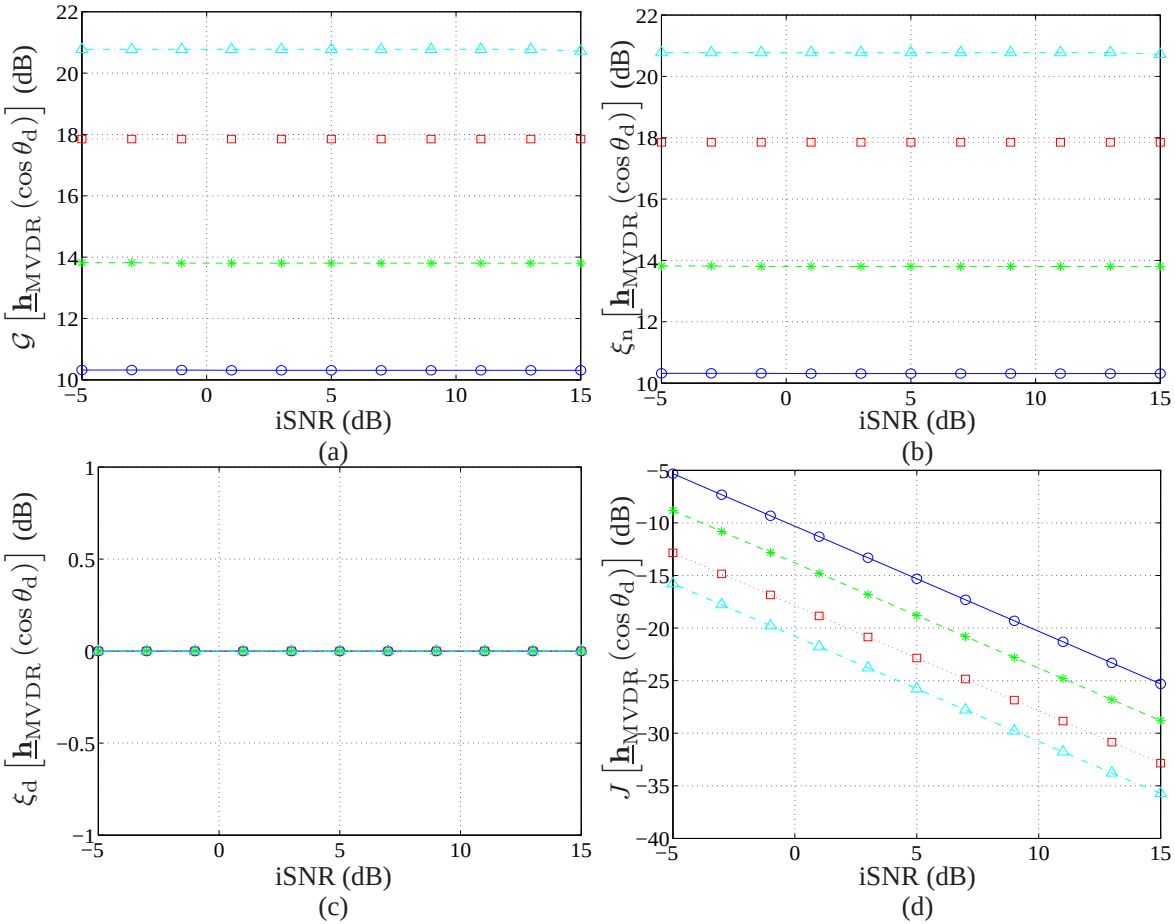

Figure 20: (a) The array gain, (b) the noise reduction factor, (c) the desired-signal reduction factor, and (d) the MSE of the MVDR beamformer for: $M = 4$ (solid line with circles), $M = 6$ (dashed line with asterisks), $M = 10$ (dotted line with squares), and $M = 15$ (dash-dot line with triangles).

Figure 21 shows broadband beampatterns, $|\mathcal{B}\left[\underline{\mathbf{h}}_{\mathrm{MVDR}}\left(\cos\theta_{\mathrm{d}}\right),\cos\theta\right]|$, for different numbers of sensors, M.

The main beam is in the direction of the desired-signal, i.e., θ_{d}, and there is a null in the direction of the interference, i.e., θ_{n}.

As the number of sensors increases, the width of the main beam decreases, the null in the direction of the interference becomes deeper, and the level of the sidelobe decreases.

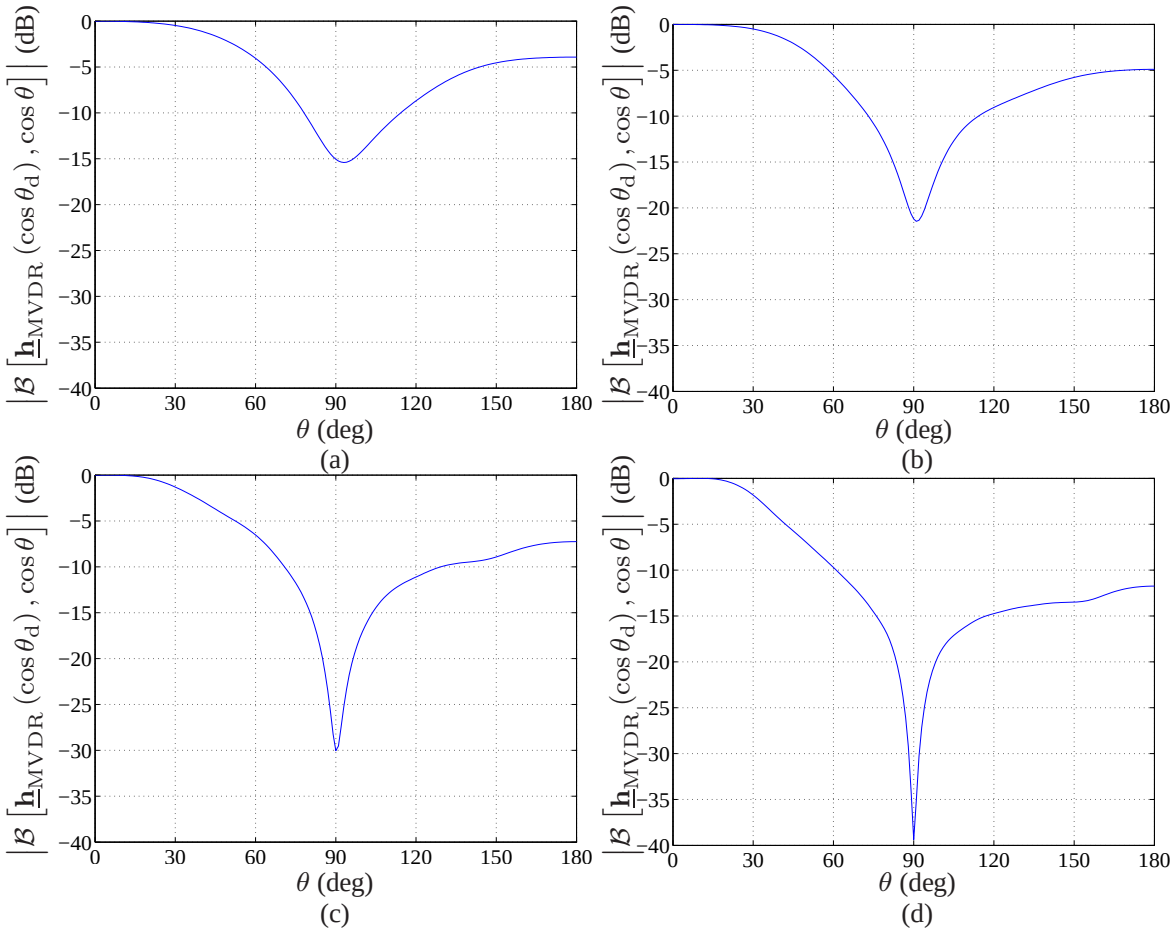

Figure 21: Broadband beampatterns of the MVDR beamformer for different numbers of sensors, M: (a) $M = 4$, (b) $M = 6$, (c) $M = 10$, and (d) $M = 15$.

Tradeoff

The easiest way to compromise between desired-signal distortion and noise reduction is to optimize the criterion:

$$\min_{\underline{\mathbf{h}}} J_{\mathrm{d}}\left(\underline{\mathbf{h}}\right) \quad \text{subject to} \quad J_{\mathrm{n}}\left(\underline{\mathbf{h}}\right) = \aleph \sigma_{v_1}^2, \tag{83}$$

where $0 < \aleph < 1$ to insure that we get some noise reduction.

By using a Lagrange multiplier, $\mu > 0$, to adjoin the constraint to the cost function, we get the tradeoff beamformer:

$$\underline{\mathbf{h}}_{\mathrm{T},\mu}\left(\cos\theta_{\mathrm{d}}\right) = \mathbf{R}_{\underline{\mathbf{v}}}^{-1}\underline{\mathbf{G}}\left(\cos\theta_{\mathrm{d}}\right) \times \left[\mu\mathbf{R}_{\mathbf{x}}^{-1} + \underline{\mathbf{G}}^{T}\left(\cos\theta_{\mathrm{d}}\right)\mathbf{R}_{\underline{\mathbf{v}}}^{-1}\underline{\mathbf{G}}\left(\cos\theta_{\mathrm{d}}\right)\right]^{-1}\mathbf{i}_{l}. \tag{84}$$

We can see that for

- $\mu = 1$, $\underline{\mathbf{h}}_{\mathrm{T},1}\left(\cos\theta_{\mathrm{d}}\right) = \underline{\mathbf{h}}_{\mathrm{W}}\left(\cos\theta_{\mathrm{d}}\right)$, which is the Wiener beamformer;
- $\mu = 0$, $\underline{\mathbf{h}}_{\mathrm{T},0}\left(\cos\theta_{\mathrm{d}}\right) = \underline{\mathbf{h}}_{\mathrm{MVDR}}\left(\cos\theta_{\mathrm{d}}\right)$, which is the MVDR beamformer;
- $\mu > 1$, results in a beamformer with low residual noise at the expense of high desired-signal distortion (as compared to Wiener); and
- $\mu < 1$, results in a beamformer with high residual noise and low desired-signal distortion (as compared to Wiener).

Example 7

Returning to Example 5, we now employ the tradeoff beamformer, $\underline{\mathbf{h}}_{\mathrm{T},\mu}\left(\cos\theta_{\mathrm{d}}\right)$, given in (84).

Figure 22 shows plots of the array gain, $\mathcal{G}\left[\underline{\mathbf{h}}_{\mathrm{T},\mu}\left(\cos\theta_{\mathrm{d}}\right)\right]$, the noise reduction factor, $\xi_{\mathrm{n}}\left[\underline{\mathbf{h}}_{\mathrm{T},\mu}\left(\cos\theta_{\mathrm{d}}\right)\right]$, the desired-signal reduction factor, $\xi_{\mathrm{d}}\left[\underline{\mathbf{h}}_{\mathrm{T},\mu}\left(\cos\theta_{\mathrm{d}}\right)\right]$, and the desired-signal distortion index, $\upsilon_{\mathrm{d}}\left[\underline{\mathbf{h}}_{\mathrm{T},\mu}\left(\cos\theta_{\mathrm{d}}\right)\right]$, as a function of the input SNR, for $M = 10$ and several values of μ.

For a given input SNR, the higher is the value of μ, the higher are the array gain and the noise reduction factor, but at the expense of higher desired-signal reduction factor and higher desired-signal distortion index.

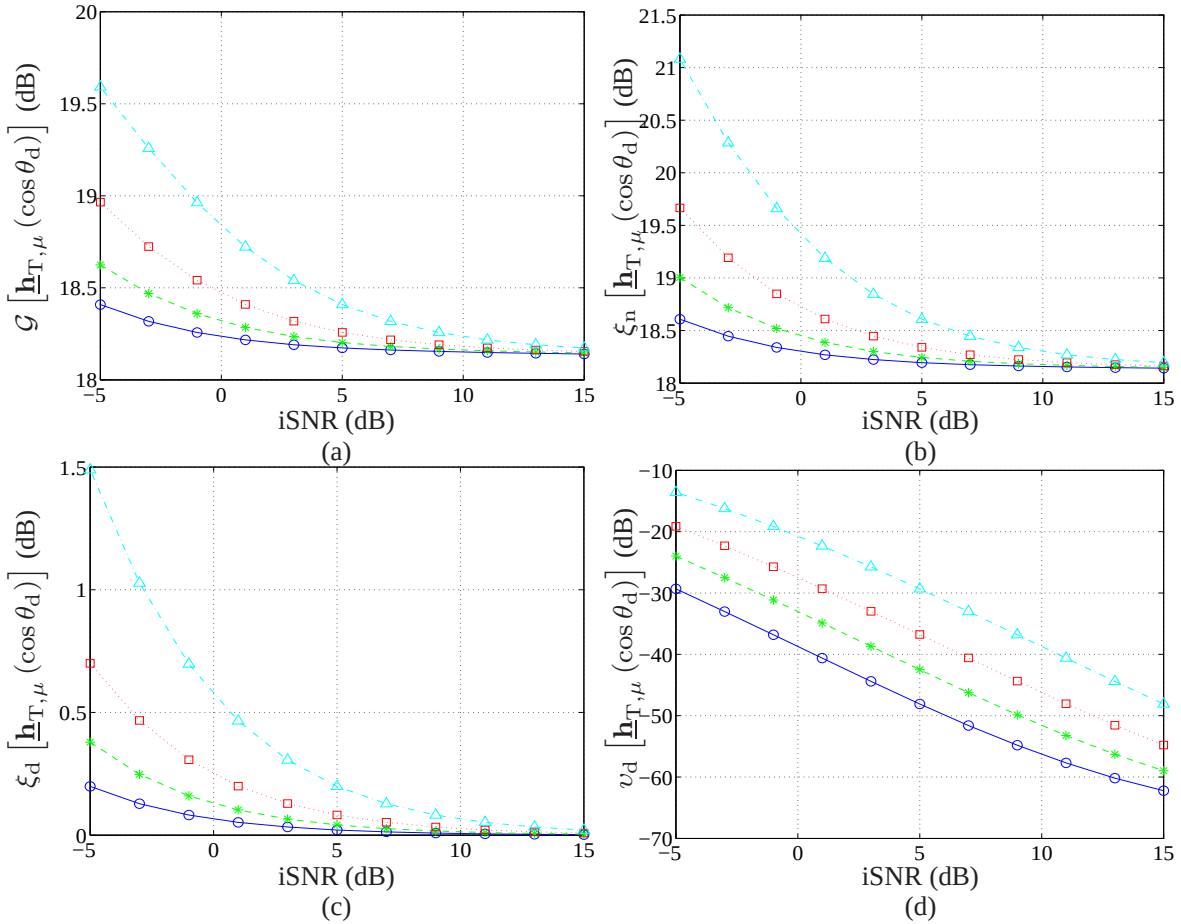

Figure 22: (a) The array gain, (b) the noise reduction factor, (c) the desired-signal reduction factor, and (d) the desired-signal distortion index of the tradeoff beamformer for $M = 10$ and for: $\mu = 0.5$ (solid line with circles), $\mu = 1$ (dashed line with asterisks), $\mu = 2$ (dotted line with squares), and $\mu = 5$ (dash-dot line with triangles).

Figure 23 shows broadband beampatterns, $\left|\mathcal{B}\left[\underline{\mathbf{h}}_{\mathrm{T},\mu}\left(\cos\theta_{\mathrm{d}}\right),\cos\theta\right]\right|$, for $M=10$ and several values of μ.

The main beam is in the direction of the desired signal, i.e., θ_{d}, and there is a null in the direction of the interference, i.e., θ_{n}.

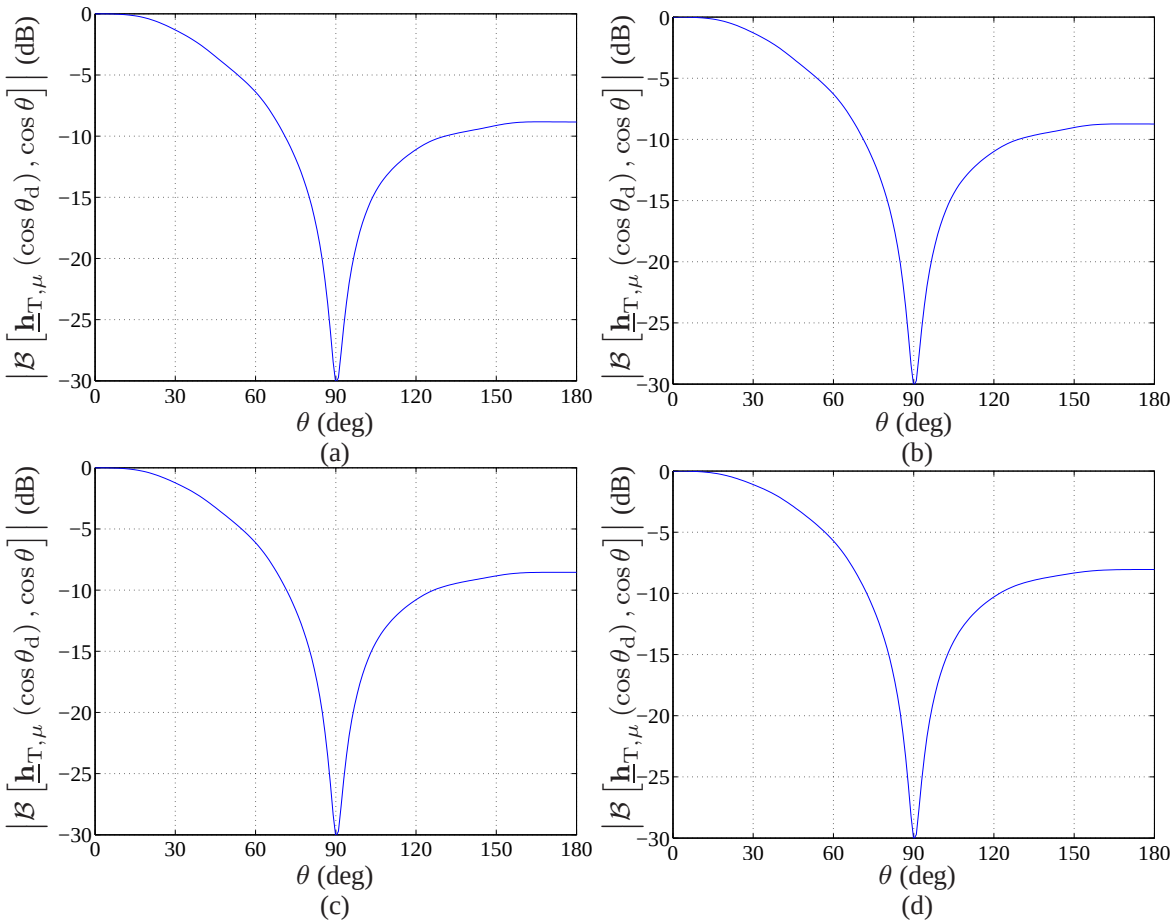

Figure 23: Broadband beampatterns of the tradeoff beamformer for $M = 10$ and several values of μ: (a) $\mu = 0.5$, (b) $\mu = 1$, (c) $\mu = 2$, and (d) $\mu = 5$.

Maximum SNR

Let us denote by $\underline{\mathbf{t}}_1'\left(\cos\theta_{\mathrm{d}}\right)$ the eigenvector corresponding to the maximum eigenvalue, $\underline{\lambda}_1'\left(\cos\theta_{\mathrm{d}}\right)$, of the matrix $\mathbf{R}_{\underline{\mathbf{v}}}^{-1}\underline{\mathbf{G}}\left(\cos\theta_{\mathrm{d}}\right)\mathbf{R}_{\mathbf{x}}\underline{\mathbf{G}}^{T}\left(\cos\theta_{\mathrm{d}}\right)$.

It is clear that the beamformer:

$$\underline{\mathbf{h}}_{\max}\left(\cos\theta_{\mathrm{d}}\right)=\varsigma\underline{\mathbf{t}}_1'\left(\cos\theta_{\mathrm{d}}\right), \tag{85}$$

where $\varsigma\neq 0$ is an arbitrary real number, maximizes the output SNR [defined in (33)].

With the maximum SNR beamformer, $\underline{\mathbf{h}}_{\max}\left(\cos\theta_{\mathrm{d}}\right)$, the output SNR is

$$\mathrm{oSNR}\left[\underline{\mathbf{h}}_{\max}\left(\cos\theta_{\mathrm{d}}\right)\right]=\underline{\lambda}_1'\left(\cos\theta_{\mathrm{d}}\right) \tag{86}$$

and

$$\mathrm{oSNR}\left[\underline{\mathbf{h}}_{\max}\left(\cos\theta_{\mathrm{d}}\right)\right]\geq\mathrm{oSNR}\left(\underline{\mathbf{h}}\right),\ \forall\underline{\mathbf{h}}. \tag{87}$$

The parameter ς can be found by minimizing distortion or the MSE.

Substituting (85) into (47) we obtain

$$J\left(\underline{\mathbf{h}}\right) = \sigma_x^2 - 2\varsigma \underline{\mathbf{t}}_1'^T \left(\cos\theta_{\mathrm{d}}\right) \underline{\mathbf{G}} \left(\cos\theta_{\mathrm{d}}\right) \mathbf{R}_{\mathbf{x}} \mathbf{i}_l + \varsigma^2 \underline{\mathbf{t}}_1'^T \left(\cos\theta_{\mathrm{d}}\right) \mathbf{R}_{\underline{\mathbf{y}}} \underline{\mathbf{t}}_1' \left(\cos\theta_{\mathrm{d}}\right). \tag{88}$$

Therefore, ς that minimizes the MSE is given by

$$\varsigma = \frac{\underline{\mathbf{t}}_1'^T \left(\cos\theta_{\mathrm{d}}\right) \underline{\mathbf{G}} \left(\cos\theta_{\mathrm{d}}\right) \mathbf{R}_{\mathbf{x}} \mathbf{i}_l}{\underline{\mathbf{t}}_1'^T \left(\cos\theta_{\mathrm{d}}\right) \mathbf{R}_{\underline{\mathbf{y}}} \underline{\mathbf{t}}_1' \left(\cos\theta_{\mathrm{d}}\right)}. \tag{89}$$

Example 8

Returning to Example 5, we now employ the maximum SNR beamformer, $\underline{\mathbf{h}}_{\max}(\cos\theta_{\mathrm{d}})$, given in (85) with ς that minimizes the MSE.

Figure 24 shows plots of the array gain, $\mathcal{G}[\underline{\mathbf{h}}_{\max}(\cos\theta_{\mathrm{d}})]$, the noise reduction factor, $\xi_{\mathrm{n}}[\underline{\mathbf{h}}_{\max}(\cos\theta_{\mathrm{d}})]$, the desired-signal reduction factor, $\xi_{\mathrm{d}}[\underline{\mathbf{h}}_{\max}(\cos\theta_{\mathrm{d}})]$, and the desired-signal distortion index, $\upsilon_{\mathrm{d}}[\underline{\mathbf{h}}_{\max}(\cos\theta_{\mathrm{d}})]$, as a function of the input SNR, for different numbers of sensors, M.

For a given input SNR, as the number of sensors increases, the array gain and noise reduction factor increase, while the desired-signal reduction factor and desired-signal distortion index decrease.

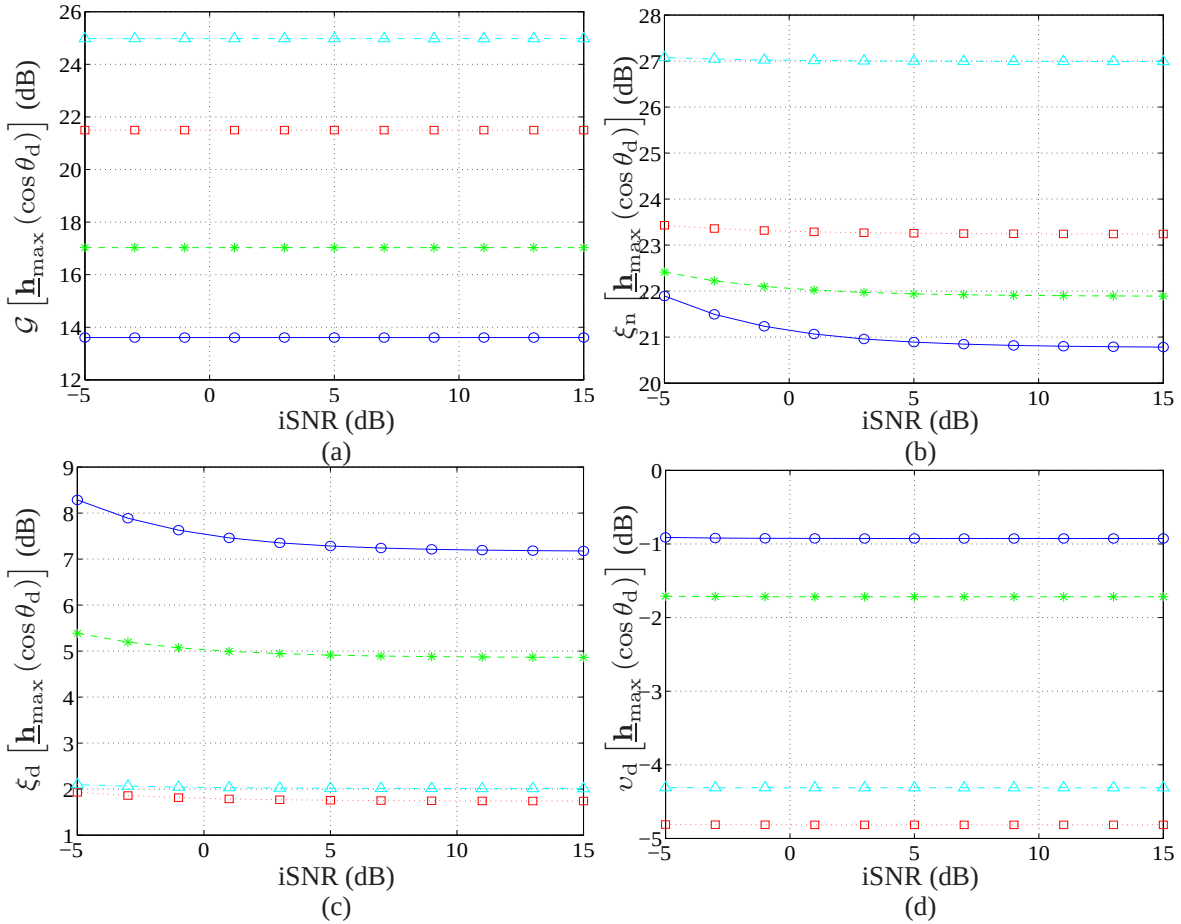

Figure 24: (a) The array gain, (b) the noise reduction factor, (c) the desired-signal reduction factor, and (d) the desired-signal distortion index of the maximum SNR beamformer for: $M = 4$ (solid line with circles), $M = 6$ (dashed line with asterisks), $M = 10$ (dotted line with squares), and $M = 15$ (dash-dot line with triangles).

Figure 25 shows broadband beampatterns, $|\mathcal{B}\left[\underline{\mathbf{h}}_{\max}\left(\cos\theta_{\mathrm{d}}\right),\cos\theta\right]|$, for different numbers of sensors, M.

The main beam is in the direction of the desired signal, i.e., θ_{d}, and there is a null in the direction of the interference, i.e., θ_{n}.

As the number of sensors increases, the null in the direction of the interference becomes deeper.

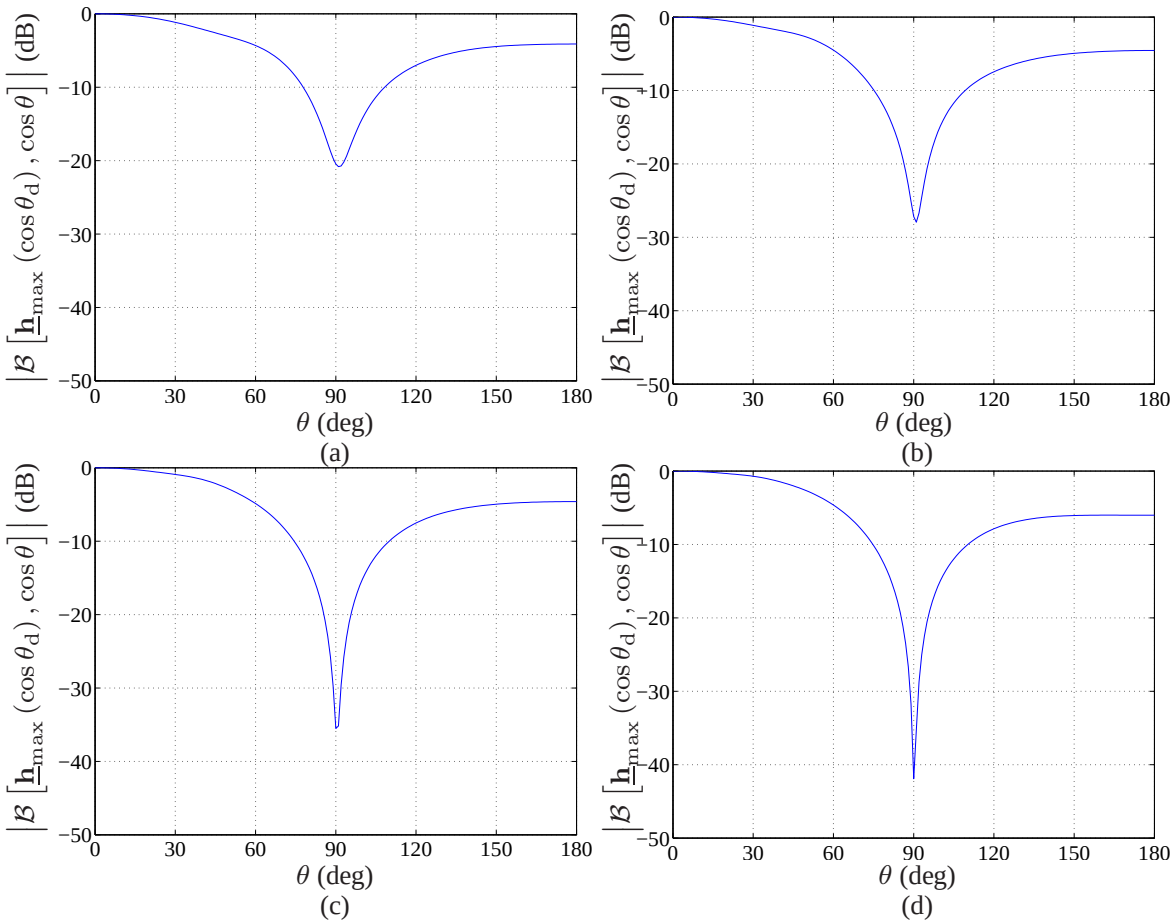

Figure 25: Broadband beampatterns of the maximum SNR beamformer for different numbers of sensors, M: (a) $M = 4$, (b) $M = 6$, (c) $M = 10$, and (d) $M = 15$.

LCMV

We assume that we have an undesired source impinging on the array from the direction $\theta_{\mathrm{n}} \neq \theta_{\mathrm{d}}$.

The objective is to completely cancel this source while recovering the desired source impinging on the array from the direction θ_{d}.

Then, it is obvious that the constraint equation is identical to the one given in (69).

The above problem is solved by minimizing the MSE of the residual noise, $J_{\mathrm{r}}\left(\underline{\mathbf{h}}\right)$, subject (69), i.e.,

$$\min_{\underline{\mathbf{h}}} \underline{\mathbf{h}}^T \mathbf{R}_{\underline{\mathbf{v}}} \underline{\mathbf{h}} \quad \text{subject to} \quad \underline{\mathbf{C}}^T\left(\theta_{\mathrm{d}}, \theta_{\mathrm{n}}\right) \underline{\mathbf{h}} = \begin{bmatrix} \mathbf{i}_l \\ \mathbf{0} \end{bmatrix} \tag{90}$$

The solution to this optimization problem gives the well-known LCMV beamformer [6], [7]:

$$\underline{\mathbf{h}}_{\mathrm{LCMV}}\left(\cos\theta_{\mathrm{d}}\right)=\mathbf{R}_{\underline{\mathbf{v}}}^{-1}\underline{\mathbf{C}}\left(\theta_{\mathrm{d}},\theta_{\mathrm{n}}\right)\times \left[\underline{\mathbf{C}}^{T}\left(\theta_{\mathrm{d}},\theta_{\mathrm{n}}\right)\mathbf{R}_{\underline{\mathbf{v}}}^{-1}\underline{\mathbf{C}}\left(\theta_{\mathrm{d}},\theta_{\mathrm{n}}\right)\right]^{-1}\begin{bmatrix}\mathbf{i}_{l}\\ \mathbf{0}\end{bmatrix}, \tag{91}$$

which depends on the statistics of the noise only.

It can be shown that a more interesting formulation of the LCMV beamformer is

$$\underline{\mathbf{h}}_{\mathrm{LCMV}}\left(\cos\theta_{\mathrm{d}}\right)=\mathbf{R}_{\underline{\mathbf{y}}}^{-1}\underline{\mathbf{C}}\left(\theta_{\mathrm{d}},\theta_{\mathrm{n}}\right)\times \left[\underline{\mathbf{C}}^{T}\left(\theta_{\mathrm{d}},\theta_{\mathrm{n}}\right)\mathbf{R}_{\underline{\mathbf{y}}}^{-1}\underline{\mathbf{C}}\left(\theta_{\mathrm{d}},\theta_{\mathrm{n}}\right)\right]^{-1}\begin{bmatrix}\mathbf{i}_{l}\\ \mathbf{0}\end{bmatrix}. \tag{92}$$

The previous expression depends on the statistics of the observations only, which should be easy to estimate.

Example 9

Returning to Example 5, we now employ the LCMV beamformer, $\underline{\mathbf{h}}_{\mathrm{LCMV}}\left(\cos\theta_{\mathrm{d}}\right)$, given in (92).

Figure 26 shows plots of the array gain, $\mathcal{G}\left[\underline{\mathbf{h}}_{\mathrm{LCMV}}\left(\cos\theta_{\mathrm{d}}\right)\right]$, the noise reduction factor, $\xi_{\mathrm{n}}\left[\underline{\mathbf{h}}_{\mathrm{LCMV}}\left(\cos\theta_{\mathrm{d}}\right)\right]$, the desired-signal reduction factor, $\xi_{\mathrm{d}}\left[\underline{\mathbf{h}}_{\mathrm{LCMV}}\left(\cos\theta_{\mathrm{d}}\right)\right]$, and the MSE, $J\left[\underline{\mathbf{h}}_{\mathrm{LCMV}}\left(\cos\theta_{\mathrm{d}}\right)\right]$, as a function of the input SNR, for different numbers of sensors, M.

For a given input SNR, as the number of sensors increases, the array gain and the noise reduction factor slightly increase.

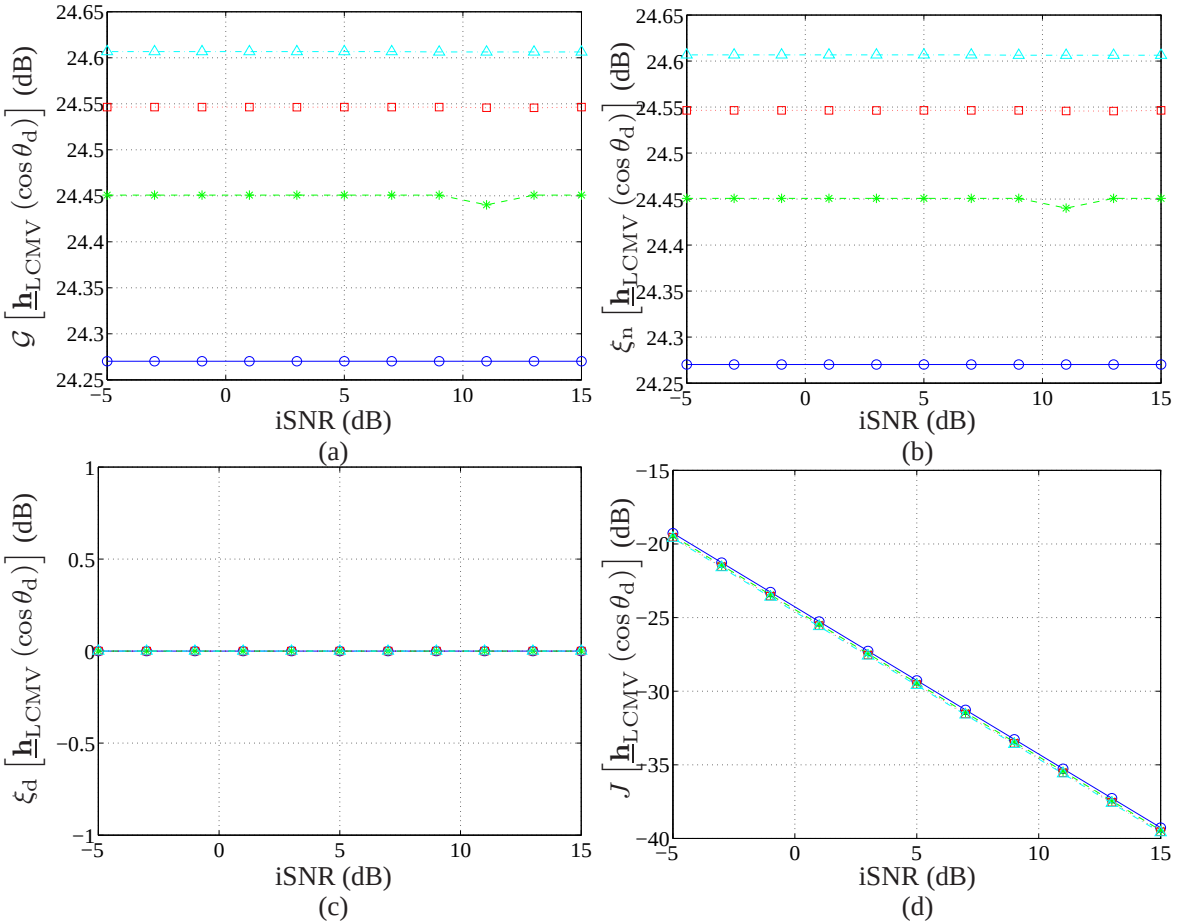

Figure 26: (a) The array gain, (b) the noise reduction factor, (c) the desired-signal reduction factor, and (d) the MSE of the LCMV beamformer for: $M = 30$ (solid line with circles), $M = 35$ (dashed line with asterisks), $M = 40$ (dotted line with squares), and $M = 45$ (dash-dot line with triangles).

Figure 27 shows broadband beampatterns, $|\mathcal{B}\left[\underline{\mathbf{h}}_{\mathrm{LCMV}}\left(\cos\theta_{\mathrm{d}}\right),\cos\theta\right]|$, for different numbers of sensors, M.

The main beam is in the direction of the desired signal, i.e., θ_{d}, and there is a null in the direction of the interference, i.e., θ_{n}. In particular, $|\mathcal{B}\left[\underline{\mathbf{h}}_{\mathrm{LCMV}}\left(\cos\theta_{\mathrm{d}}\right),\cos\theta\right]|$ is 1 for $\theta=\theta_{\mathrm{d}}$, and is identically zero for θ_{n}.

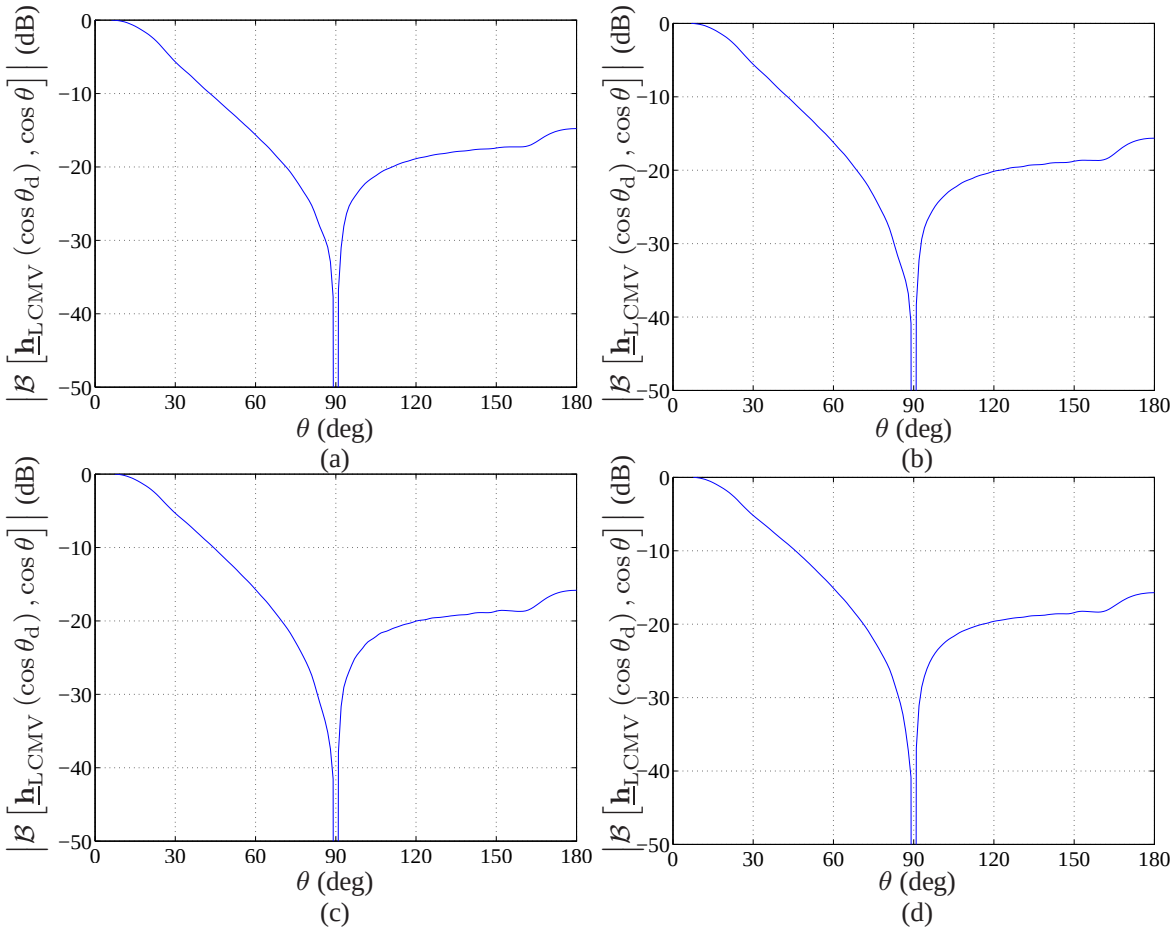

Figure 27: Broadband beampatterns of the LCMV beamformer for different numbers of sensors, M: (a) $M = 30$, (b) $M = 35$, (c) $M = 40$, and (d) $M = 45$.

In Table 2, we summarize all the time-domain adaptive beamformers derived in this section.

Table 2: Adaptive beamformers in the time domain.

Wiener:	$\underline{\mathbf{h}}_{\mathrm{W}}(\cos\theta_{\mathrm{d}}) = \mathbf{R}_{\underline{\mathbf{v}}}^{-1}\underline{\mathbf{G}}(\cos\theta_{\mathrm{d}}) \times \left[\mathbf{R}_{\mathbf{x}}^{-1} + \underline{\mathbf{G}}^{T}(\cos\theta_{\mathrm{d}})\mathbf{R}_{\underline{\mathbf{v}}}^{-1}\underline{\mathbf{G}}(\cos\theta_{\mathrm{d}})\right]^{-1}\mathbf{i}_l$
MVDR:	$\underline{\mathbf{h}}_{\mathrm{MVDR}}(\cos\theta_{\mathrm{d}}) = \mathbf{R}_{\underline{\mathbf{v}}}^{-1}\underline{\mathbf{G}}(\cos\theta_{\mathrm{d}}) \times \left[\underline{\mathbf{G}}^{T}(\cos\theta_{\mathrm{d}})\mathbf{R}_{\underline{\mathbf{v}}}^{-1}\underline{\mathbf{G}}(\cos\theta_{\mathrm{d}})\right]^{-1}\mathbf{i}_l$
Tradeoff:	$\underline{\mathbf{h}}_{\mathrm{T},\mu}(\cos\theta_{\mathrm{d}}) = \mathbf{R}_{\underline{\mathbf{v}}}^{-1}\underline{\mathbf{G}}(\cos\theta_{\mathrm{d}}) \times \left[\mu\mathbf{R}_{\mathbf{x}}^{-1} + \underline{\mathbf{G}}^{T}(\cos\theta_{\mathrm{d}})\mathbf{R}_{\underline{\mathbf{v}}}^{-1}\underline{\mathbf{G}}(\cos\theta_{\mathrm{d}})\right]^{-1}\mathbf{i}_l,\ \mu \geq 0$
Max. SNR:	$\underline{\mathbf{h}}_{\max}(\cos\theta_{\mathrm{d}}) = \varsigma\underline{\mathbf{t}}_1'(\cos\theta_{\mathrm{d}}),\ \varsigma \neq 0$
LCMV:	$\underline{\mathbf{h}}_{\mathrm{LCMV}}(\cos\theta_{\mathrm{d}}) = \mathbf{R}_{\underline{\mathbf{v}}}^{-1}\underline{\mathbf{C}}(\theta_{\mathrm{d}},\theta_{\mathrm{n}}) \times \left[\underline{\mathbf{C}}^{T}(\theta_{\mathrm{d}},\theta_{\mathrm{n}})\mathbf{R}_{\underline{\mathbf{v}}}^{-1}\underline{\mathbf{C}}(\theta_{\mathrm{d}},\theta_{\mathrm{n}})\right]^{-1}\begin{bmatrix}\mathbf{i}_l \\ \mathbf{0}\end{bmatrix}$

[1] J. Benesty, J. Chen, and Y. Huang, *Microphone Array Signal Processing*. Berlin, Germany: Springer-Verlag, 2008.

[2] C. E. Shannon, “Communications in the presence of noise,” *Proc. IRE*, vol. 37, pp. 10–21, 1949.

[3] A. J. Jerri, “The Shannon sampling theorem. Its various extensions and applications: a tutorial review,” *Proc. IEEE*, vol. 65, pp. 1565–1596, Nov. 1977

[4] H. Cox, R. M. Zeskind, and T. Kooij, “Practical supergain,” *IEEE Trans. Acoust., Speech, Signal Process.*, vol. ASSP-34, pp. 393–398, June 1986.

[5] H. Cox, R. M. Zeskind, and M. M. Owen, “Robust adaptive beamforming,” *IEEE Trans. Acoust., Speech, Signal Process.*, vol. ASSP-35, pp. 1365–1376, Oct. 1987.

[6] A. Booker and C. Y. Ong, “Multiple constraint adaptive filtering,” *Geophysics*, vol. 36, pp. 498–509, June 1971.

[7] O. Frost, “An algorithm for linearly constrained adaptive array processing,” *Proc. IEEE*, vol. 60, pp. 926–935, Jan. 1972.

[8] J. Benesty and J. Chen, *Study and Design of Differential Microphone Arrays*. Berlin, Germany: Springer-Verlag, 2012.

[9] G. W. Elko, “Superdirectional microphone arrays,” in *Acoustic Signal Processing for Telecommunication*, S. L. Gay and J. Benesty, Eds. Boston, MA: Kluwer Academic Publishers, 2000, Chapter 10, pp. 181–237.

[10] R. N. Marshall and W. R. Harry, “A new microphone providing uniform directivity over an extended frequency range,” *J. Acoust. Soc. Am.*, vol. 12, pp. 481–497, 1941.